haematologica
Journal of the Ferrata Storti Foundation

NFATc1 and NFATc2 regulate glucocorticoid resistance in pediatric T-cell acute lymphoblastic leukemia through modulation of cholesterol biosynthesis and the WNT/β-catenin pathway

by Giulia Veltri, Alberto Peloso, Alice Cani, Elena Mariotto, Diana Corallo, Sanja Aveic, Loris Russo, Matilde Cescon, Giulia Santinon, Chiara Frasson, Katharina Simon, Alberto Arrighi, Egidio Iorio, Sonia Anna Minuzzo, Stefano Indraccolo, Sandra Marmiroli, Panagiotis Ntziachristos, Alessandra Biffi, Martina Pigazzi, Barbara Buldini, Silvia Bresolin and Valentina Serafin

Received: February 28, 2025.
Accepted: September 24, 2025.

Citation: Giulia Veltri, Alberto Peloso, Alice Cani, Elena Mariotto, Diana Corallo, Sanja Aveic, Loris Russo, Matilde Cescon, Giulia Santinon, Chiara Frasson, Katharina Simon, Alberto Arrighi, Egidio Iorio, Sonia Anna Minuzzo, Stefano Indraccolo, Sandra Marmiroli, Panagiotis Ntziachristos, Alessandra Biffi, Martina Pigazzi, Barbara Buldini, Silvia Bresolin and Valentina Serafin. NFATc1 and NFATc2 regulate glucocorticoid resistance in pediatric T-cell acute lymphoblastic leukemia through modulation of cholesterol biosynthesis and the WNT/β-catenin pathway.
Haematologica. 2025 Oct 2. doi: 10.3324/haematol.2025.287651 [Epub ahead of print]

Publisher's Disclaimer.
E-publishing ahead of print is increasingly important for the rapid dissemination of science. Haematologica is, therefore, E-publishing PDF files of an early version of manuscripts that have completed a regular peer review and have been accepted for publication.
E-publishing of this PDF file has been approved by the authors.
After having E-published Ahead of Print, manuscripts will then undergo technical and English editing, typesetting, proof correction and be presented for the authors' final approval; the final version of the manuscript will then appear in a regular issue of the journal.
All legal disclaimers that apply to the journal also pertain to this production process.

NFATc1 and NFATc2 regulate glucocorticoid resistance in pediatric T-cell acute lymphoblastic leukemia through modulation of cholesterol biosynthesis and the WNT/β-catenin pathway

Giulia Veltri[1,2], Alberto Peloso[1,2], Alice Cani[1,2], Elena Mariotto[1,2], Diana Corallo[2-3], Sanja Aveic[3], Loris Russo[4], Matilde Cescon[4], Giulia Santinon[1,2], Chiara Frasson[2], Katharina Simon[1,5], Alberto Arrighi[1,2], Egidio Iorio[6], Sonia Anna Minuzzo[7], Stefano Indraccolo[7,8], Sandra Marmiroli[9], Panagiotis Ntziachristos[10-12], Alessandra Biffi[1,2], Martina Pigazzi[1,2], Barbara Buldini[1,2], Silvia Bresolin[1,2] and Valentina Serafin[2,9*]

(1) Division of Pediatric Hematology, Oncology and Stem Cell Transplant, Maternal and Child Health Department, University of Padova, Padova, Italy;
(2) Pediatric Research Institute Città della Speranza Foundation, Padova, Italy;
(3) Laboratory of Target Discovery and Biology of Neuroblastoma, Pediatric Research Institute Città della Speranza Foundation, Padova, Italy;
(4) Department of Molecular Medicine, University of Padova, Padova, Italy;
(5) Department of Pharmaceutical and Pharmacological Sciences, University of Padova, Padova, Italy;
(6) High Resolution NMR Unit Core Facilities Istituto Superiore Di Sanità, Roma, Italy;
(7) Department of Surgery, Oncology and Gastroenterology, University of Padova, Padova, Italy;
(8) Basic and Translational Oncology Unit, Veneto Institute of Oncology IOV - IRCCS, Padova, Italy;
(9) Cellular Signaling Unit, Department of Biomedical, Metabolic and Neural Sciences, University of Modena and Reggio Emilia, Modena, Italy;
(10) Leukemia Therapy Resistance Lab, Department of Biomolecular Medicine, Faculty of Medicine and Health Sciences, Ghent University – Ghent, Belgium;
(11) Cancer Research Institute Ghent (CRIG) – Ghent, Belgium;
(12) Center for Medical Genetics Ghent (CMGG) – Ghent, Belgium.

Author contributions

GV designed the study, performed, interpreted most of the experiments and wrote the manuscript. AP performed all the bioinformatic analyses and contributed to the writing and reviewing of the manuscript. AC performed all the transcriptomic experiments and contributed to the writing and reviewing of the manuscript. EM performed all the HTS experiments and statistical analyses. DC and SA performed *in vivo* experiments and data analysis. LR performed immunofluorescence analysis and MC supervised the analysis. GS performed lentiviral design and production. CF performed cytofluorimetric assays and analysis. KS and AA performed experiments. EI is responsible for NMR analysis. SAM and SI provided primary T-ALL cells from PDX mice. SM, PN, MP, and AB support with resources and writing editing. BB contributes with pathology review. SB contributes to conceptualization, and she supervised the transcriptome analysis, writing–review and editing. VS conceptualized, designed and supervised the study, acquired fundings, managed the project and wrote the original draft of the manuscript.

Running Heads: NFATc1/c2 as new glucocorticoid resistance drivers

Corresponding Author: Valentina Serafin email: valentina.serafin@unimore.it

ORCID: https://orcid.org/0000-0001-6283-7728

Data-sharing statement
The study utilized, in part, publicly available datasets (Haferlach T, et al. J Clin Oncol. 2010;28(15):2529-37). The gene expression data sets generated during this study are available at the Gene Expression Omnibus database under accession number GSE254001 and/or in the Supplementary Materials. Derived data supporting the findings of this study are available from the corresponding author upon reasonable request.

Word count. Abstract 250 words. Main Text 4276 words. Six main figures are in the manuscript. One supplementary file is associated with the manuscript.

Acknowledgments
We gratefully acknowledge the informative discussions with Dr. B. Accordi, Dr. G. Borile and Dr. V. Conter.

Founding
VS is supported by the Fondazione Associazione Italiana per la Ricerca sul Cancro (AIRC, MFAG 2018, ID 21771) and by the Associazione italiana contro le leucemie-linfomi e mieloma (AIL)-TV. VS was also supported by Fondazione Umberto Veronesi (FUV) (#2954). GV by AIRC (ID 29579). AC by FUV (#4420, #4820, #5216, #5581), EM by STARS@UNIPD (ID "STUMBLE"), and Istituto di Ricerca Pediatrica Città della Speranza (#24/12 IRP) and FUV (#5318), DC by FUV (#5260), SB by AIRC IG (ID 27168) and Fondazione Cariparo 20/12. MC is funded by Italian Ministry of University and Research and European Union (P2022Y2A3L, CUP C53D23007520001; 20227YB93W, CUP C53D23003030001; Next Generation EU, Project CN00000041, CUP B93D21010860004, Spoke n. 5) and by Telethon-AFM (#28703). SM was supported by Associazione Mantovana per la Ricerca sul Cancro (A.Ma.Ri.Ca) 2024 E93C24000290007 and by FAR FOMO 2022 Mission Oriented E93C22000800007. BB by Fondazione Cariparo (20/12_FCR). The PN group is supported by the Research Foundation Flander (G0F4721N, and G0A8B24N), The Foundation against Cancer (F/2024/2666), start-up funds from the Department of Biomolecular Medicine, Ghent University, a Flanders Interuniversity Consortium Grant (BOF.IBO.2023.0006.02) and a Cancer Research Institute Ghent partnership grant.

Conflict of interest statement
The authors declare that they have no conflict of interest.

Abstract

The glucocorticoid (GC) resistance onset in pediatric T-cell Acute Lymphoblastic Leukemia (T-ALL) patients remains one of the biggest challenges in current cancer treatment. The mechanisms driving this resistance are still not fully understood, making it difficult to predict patient outcomes and to develop effective therapies. Our study uncovered critical insights into the biological processes underlying GC resistance, offering potential breakthroughs for future treatments. Building on our previous research on LCK kinase hyperactivation in GC-resistant T-ALL patients, we have now delved deeper into the LCK downstream NFAT transcription factor family's contribution to GC resistance. We discovered that, even at the time of diagnosis, GC resistant T-ALL patients exhibit an intrinsic low glucocorticoid receptor (GR) activity coupled with high NFATc1 and NFATc2 ones. This dysregulation creates a roadblock to effective GC therapy. Indeed, in the absence of either NFATc1 or NFATc2, the normal transcriptional activity of GR is restored, re-sensitizing the leukemia cells to dexamethasone treatment both *in vitro* and *in vivo*. This suggests that NFATc1 and NFATc2 are central to driving GC resistance, as they directly regulate crucial pathways like cholesterol biosynthesis and WNT/β-catenin signaling. The identification of NFAT transcription factors as key players in leukemia therapy resistance offers a promising target for future therapeutic strategies, potentially transforming the way we approach treatment for these challenging conditions or autoimmune disorders where glucocorticoids are a cornerstone of treatment.

Abbreviation sentence

This study explores the mechanisms underlying glucocorticoid resistance in pediatric T-cell Acute Lymphoblastic Leukemia (T-ALL), with a particular focus on the role of NFAT transcription factors in modulating the response of T-ALL cells to glucocorticoid treatment.
Our findings reveal that NFATc1 and NFATc2 play critical roles in driving glucocorticoid resistance by regulating cholesterol biosynthesis and WNT/β-catenin signaling, respectively.
The inhibition of these factors can restore glucocorticoid receptor activity, offering a promising avenue for the development of future therapeutic strategies.

Introduction

T-cell acute lymphoblastic leukemia (T-ALL) is a heterogeneous childhood malignancy characterized by an aberrant T-cell growth, proliferation, survival, and differentiation, accounting for 10-15% of all pediatric ALL cases [1]. Glucocorticoids (GC), such as dexamethasone (dex), due to their immunosuppressive and anti-inflammatory effects on immune cells, are pillar drugs of T-ALL pediatric patients' multi-agent therapeutic protocol[2]. These compounds exert their genomic pro-apoptotic effects via the Glucocorticoid Receptor (GR), a ligand-activated protein and member of the nuclear receptor superfamily of transcription factors [3,4]. Notably, the GC resistance onset after the first 8 days of treatment and the minimal residual disease (MRD) detection on day +78 $\geq 10^{-3}$, still represent the strongest predictors of poor treatment outcome [5,6]. Indeed, it is well reported that although GC resistant patients, namely Prednisone Poor Responder (PPR), are assigned to the High Risk (HR) arm of the protocol, they tend to have a worse prognosis compared to the other T-ALL HR patients [5-7]. Recently, the hyperactivation of the Lymphocyte Cell-Specific Protein-Tyrosine Kinase (LCK), which is activated downstream of the T-Cell Receptor (TCR), has been associated in ALL with GC resistance by our group and other authors [8-11]. Furthermore, we found that genes belonging to the Nuclear Factor of Activated T cells (NFAT) family, which is downstream LCK kinase, are enriched in diagnosed PPR T-ALL patients [8]. NFAT is a family of five different transcription factors, of which the first four are activated by the Ca^{2+}/calmodulin-dependent phosphatase calcineurin. In resting conditions, the NFAT proteins are heavily phosphorylated and reside in the cytoplasm of T cells. Following the TCR engagement and LCK activation, T-cells are stimulated by a rise in intracellular Ca^{2+} level, following NFAT proteins are dephosphorylated by calcineurin and translocated to the nucleus to activate target genes expression [12]. On the contrary, NFAT activity is inhibited by several kinases, including glycogen-synthase kinase 3, casein kinase 1, p38 and JUN N-terminal kinase, that by phosphorylating NFAT proteins, they control their nuclear shuttling [13]. Notably, the Calcineurin/NFAT signaling pathway, which is fundamental to maintaining normal T-cell physiology, has been found to be deregulated in B-cell lymphomas [14] and *NFATc1, NFATc2* and *NFATc3* have been reported in T-ALL initiating potential and progression [15-17]. Despite this, the mechanisms behind the LCK/NFAT-driven GC resistance remain to be elucidated in T-ALL pediatric patients. Our study is the first to report how the NFAT transcription factors, particularly NFATc1 and NFATc2, drive GC resistance in T-ALL. Already at diagnosis, GC-resistant T-ALL patients exhibit an intrinsic imbalance; high levels of NFATc1 and NFATc2 activity coupled with low GR transcriptional activity. This imbalance is not just a marker of GC resistance but a key mechanism that underpins it. We found that these NFAT factors directly interfere with GR function by regulating two critical pathways: cholesterol biosynthesis and the WNT/β-catenin whose inhibition restores GR activity and sensitize T-ALL cells to dexamethasone treatment. The implications of our findings are profound. By unlocking the mechanisms that drive GC resistance in T-ALL, we not only gain a deeper understanding of the disease but also open the door to more effective therapies. Targeting the NFAT-driven pathways or even NFAT directly could lead to new, more personalized treatment options for pediatric T-ALL patients, ultimately improving survival rates and outcomes for children battling this aggressive form of leukemia.

Methods

Transcriptome data analysis

Transcriptome data from 104 T-ALL pediatric patients at diagnosis, belonging to the AIEOP-BFM ALL2000/R2006 therapeutic protocol were available [18,19]. NetBID2 [20], a data-driven network-based inference pipeline was applied to identify driver transcription factors (TFs) and signaling factors (SIGs) in T-ALL patients (see Extended methods).

High-Throughput drug synergism screening (HTS)
HTS was conducted on primary T-ALL cells from PDXs and GC-resistant T-ALL cell lines using a 6×6 dose matrix of drugs (Cyclosporin A (CsA), dexamethasone, simvastatin, or PRI-724) in single or combination treatments. Cells were seeded in 384-well plates, pre-treated 24 hours with drugs followed by dex. After 48 hours, viability was assessed via resazurin assay. Data were normalized and analyzed for drug synergy using the SynergyFinder R package (see Extended methods).

Annexin V/Propidium Iodide staining
Cell death was assessed using Annexin V–FLUOS staining (Roche) in cell lines and primary cells treated with CsA, simvastatin, PRI-724, or dexamethasone in *NFATc1/c2*-silenced conditions (see Extended methods).

Xenotransplantation model and *in vivo* drug treatment
Two-day-old Tg(fli1:EGFP) zebrafish embryos were anesthetized and placed on agarose. TALL-1 ShRNA *NFATc1*, RPMI-8402 ShRNA *NFATc2*, and control cells were labeled with Vybrant® DIL (Invitrogen). All procedures were approved by the Italian Ministry of Health (Decree No. 21/2019-UT) and the institutional animal welfare committee (OPBA, approval No. 5168F_N03ZFU5), in compliance with D.lgs 26/2014 (see Extended methods).

3-(4,5-dimethylthiazol-2-yl)-2,5-diphenyltetrazolium bromide (MTT) assay
The effect of drug treatments or *NFATs* gene silencing on cell lines proliferation was measured using MTT assay. Cells were plated in triplicate, incubated with MTT for 4 hours, and viability was measured (see Extended methods).

GR-luciferase assays
TALL-1, ALL-SIL (ShRNA *NFATc1*/control) and RPMI-8402, LOUCY (ShRNA *NFATc2*/control) cells were electroporated with the GR-GRE-luciferase reporter and pMAXGFP vector. GFP signal was used to assess transfection efficiency and normalize luciferase activity (see Extended methods).

Filipin III staining
Intracellular cholesterol levels were measured in *NFATc1*- or *NFATc2*-silenced and control cells using the Cholesterol Cell-Based Detection Assay Kit (Cayman Chemical) (see Extended methods).

Chromatin immunoprecipitation (ChIP) and droplet digital PCR (ddPCR) analysis
ChIP was performed on TALL-1 and RPMI-8402 cells crosslinked with formaldehyde, lysed, and sonicated. Precleared chromatin was incubated with NFATc1 or NFATc2 antibodies (or IgG control). DNA was eluted, de-crosslinked, and purified. NFAT binding to selected genomic regions was assessed by ddPCR (see Extended methods).

Lipid Rafts (LRs) staining
To detect plasma membrane LRs in ALL-SIL and TALL-1 ShRNA *NFATc1* knock-down cells and controls, the Vybrant™ Alexa Fluor™ 488 Lipid Raft Labeling Kit (Thermo Fisher Scientific) was employed as detailed in the Extended methods.

LCK staining

LCK expression was assessed by immunofluorescence in ALL-SIL and TALL-1 *NFATc1*-silenced and control cells. Cells were fixed, permeabilized, and stained with primary and secondary antibodies, as detailed in the Extended methods.

Flow Cytometry

Immunophenotyping was performed on *NFATc1*- or *NFATc2*-silenced cells and respective controls. Cells were incubated with the appropriate antibody mixes for 30 minutes at room temperature, as detailed in the Extended methods.

Statistical analysis

Statistical analyses were performed using the Graphpad Prism v8 software program (GraphPad Software, La Jolla, CA) or R software packages (www.r-project.org).

Results

NFATc1 and *NFATc2* transcriptional activity and signaling negatively correlate with *GR* ones in T-ALL pediatric patients at diagnosis

To examine T-ALL GC resistance transcriptional mechanisms and identify hub drivers we applied the data-driven network-based NetBID2 tool [20] to a cohort of pediatric T-ALL patients at diagnosis, classified based on GC response [5-7]. Interestingly, among the top drivers we identified the *GC Nuclear Receptor Subfamily 3 Group C Member 1 (NR3C1)*, already known to be associated with glucocorticoid response, as well as *NFATc2* and *NFATc1*, although the latter at the limit of significance (Figure 1A). This result confirmed our previous evidence of the LCK-Calcineurin NFAT axis involvement in T-ALL GC resistance[11]. Additionally, we revealed a negative correlation between *NR3C1* transcriptional activity/signaling and *NFATc1/NFATc2* ones (Figures 1B, S1A). Furthermore, among T-ALL patients with a high *NFATc1* and/or *NFATc2* transcriptional activity/signaling and a low *NR3C1* ones we observed an enrichment of PPR patients. On the contrary, most Prednisone Good Responders (PGR) patients clustered together showing low *NFATc1* and/or *NFATc2* transcriptional activity/signaling and high *NR3C1* ones. No significant association with a specific T-ALL subtype has been observed (Figure 1C). Altogether these results suggest a putative role of NFATc1 and NFATc2 in GC response and prompted us to further investigate their function in guiding T-ALL GC resistance.

NFATc1 and NFATc2 inhibition either by CsA or by specific gene silencing re-sensitize T-ALL cells to GC treatment

First, we demonstrated the pivotal role of NFATs inhibition in sensitizing T-ALL cells to GC action by using CsA, a Food and Drug Administration approved Calcineurin/NFAT inhibitor, in combination with dex in four T-ALL GC resistant cell lines (ALL-SIL, RPMI-8402, TALL-1 and LOUCY) and in primary T-ALL cells derived from four different PDX mice models. Notably, the CsA treatment strongly synergizes with dex on reducing GC resistant cell proliferation and viability both in cell lines and in primary T-ALL cells (Figures 1D-E, S1B-D, S2A). Interestingly, we did not observe the same synergistic effect of CsA and dex combination on GC sensitive primary T-ALL cells (Figures S2B-C). Notably, among the most expressed NFAT members in T-ALL cells, CsA treatment mostly affects NFATc1 expression and activation in ALL-SIL and TALL-1, and the NFATc2 one in RPMI-8402 and LOUCY cell lines (Figures S3A-C). Additionally, a slight increase in NFATc3 was observed in nearly all the cell lines tested (Figure S3C). However, only the silencing of NFATc1 or NFATc2, following single NFATc1-c2-c3 knock-down and subsequent dexamethasone treatment, was able to restore glucocorticoid sensitivity in GC-resistant T-ALL cells (Figures S4A-C). Consistently with this

evidence, the overexpression (OE) of either *NFATc1* or *NFATc2* gene turns 720 and the 5146 GC sensitive T-ALL cell lines resistant to dex treatment (Figures S5A-D). We further validated the role of these two transcription factors both in zebrafish embryos implanted with GC resistant T-ALL cells stably silenced for either *NFATc1* or *c2* expression and treated with dex, as well as in PDXs GC resistant T-ALL primary cells. As expected, the embryos injected with TALL-1 ShRNA *NFATc1* and RPMI-8402 ShRNA *NFATc2* showed a significantly reduced number of circulating leukemia cells after dex treatment compared to controls, further highlighting the enhanced cytotoxic effect of dex in absence of either *NFATc1* or *c2 in vivo* (Figures 2A-B, S5E-G). In agreement, primary T-ALL cells silenced for either *NFATc1* or *NFATc2* expression are more susceptible to dex treatment compared to controls. (Figure 2C and S5H-I). Based on physiological evidence supporting the selective transport of steroids by ATP-binding cassette Subfamily B Member 1 (ABCB1) and its reported overexpression in the context of glucocorticoid resistance [21-23], we subsequently evaluated whether the ABCB1 transporter's downregulation could be responsible for GC sensitivity restoration. Surprisingly, we did not observe any changes in GC response using the ABC transporters inhibitor tariquidar, in combination with dex in T-ALL GC resistant cells (Figure S5L). Furthermore, the *ABCB1* mRNA expression was not decreased after *NFATc1* or *NFATc2* knock-down (Figure S5M). Overall, these results demonstrate that CsA in combination with dex can sensitize both cell lines and primary T-ALL cells to GC action and that, both *in vitro* and *in vivo*, NFATc1 and NFATc2 are the main Calcineurin/NFAT pathway players that drive GC resistance in T-ALL cells without exploiting the ABC transporters activity.

NFATc1 and NFATc2 support GC resistance in T-ALL cells by hindering the GR canonical transcriptional activity

Based on the evidence of the increased GC sensitivity in *NFATc1/c2* knock-down cells, we evaluated the impact of *NFATc1* or *NFATc2* gene silencing on GR canonical transcriptional activity. We applied the Gene Set Enrichment Analysis (GSEA) on the upregulated differentially expressed genes (DEGs) in T-ALL-1 ShRNA *NFATc1* and RPMI-8402 ShRNA *NFATc2* knock-down cells treated with dex. As expected, we observed a positive enrichment of genes related to corticosteroid response (Figure 3A). In particular, the transcription of several GR target genes such as *Interleukin-10 (IL-10), Serum/Glucocorticoid Regulated Kinase 1* (*SGK1)* and *BCL2 Like 11* (*BCL2L11)*, is restored upon dex treatment in ShRNA *NFATc1* and ShRNA *NFATc2*-expressing cells (Figure 3B). Additionally, the 43% and 40% of genes significantly upregulated by dex in *NFATc1* and *NFATc2* genes silenced cells are in common with the ones upregulated by dex in P12-ICHIKAWA GC sensitive T-ALL cell line, including genes related to GR transcriptional activity (Figure 3C). In agreement, we observed a significant increase in the GR transcriptional activity in T-ALL GC resistant cells silenced for either *NFATc1* or *NFATc2* expression and treated with dex compared to controls (Figure 3D). Altogether, these results indicate that both *NFATc1* and *NFATc2* are involved in GC response and their knock-down sensitizes GC resistant T-ALL cells to dex action by reestablishing the GR transcriptional program of a cell intrinsically sensitive to GC.

NFATc1 directly regulates cholesterol biosynthesis in GC resistant T-ALL cells

To disclose the biological processes (BPs) controlled by NFATc1 likely to be involved in driving GC resistance, we conducted transcriptome analysis in TALL-1 ShRNA *NFATc1* knock-down cells. Specifically, by applying Over Representation Analysis (ORA) of Gene Ontology for biological processes (GO-BP) on upregulated DEGs, we found the negative regulation of leukocyte activation among the most significant upregulated BPs in absence of *NFATc1* (Figure S6). Conversely, among the most significantly downregulated BPs and hallmarks in cancers in *NFATc1* knock-down condition we

found cell cycle regulation, a well-known NFATc1 target process [24,25], and cholesterol biosynthesis (Figures S7A-B). Thus, based on the emerging role of cholesterol metabolism in aggressive Early T-cell Precursor ALL (ETP-ALL) subtype and the cholesterol biosynthesis' contribution to chemotherapy resistance in different cancer cells [26-28], we deeply investigated the relationship between NFATc1 and cholesterol biosynthesis in T-ALL GC resistant cells. Firstly, by Filipin III fluorescence assay, we confirmed the specificity of the intracellular cholesterol pool decrease in *NFATc1* knock-down cells compared to controls (Figure 4A). Of note, we did not observe an equal reduction in RPMI-8402 *NFATc2* knock-down cells, thus suggesting that other BPs may be involved in NFATc2-driven GC resistance (Figure S8A). In addition, in absence of *NFATc1*, by Nuclear Magnetic Resonance (NMR) spectroscopy, we observed a significant decrease in sphingolipids, polyunsaturated fatty acids, as well as in the three cholesterol biosynthesis intermediates namely: cholestenol, lathosterol and 7-dehydrocholesterol (Figure S8B-C). Interestingly, we revealed that NFATc1 can directly bind to the DNA promoter region of the *7-Dehydrocholesterol Reductase (DHCR7), Hydroxy-3-Methylglutaryl-CoA Synthase 1 (HMGCS1), Emopamil-Binding Protein (EBP)* genes, encoding key cholesterol biosynthesis enzymes, and not to the internal negative control (IgG) and *Myogenic Differentiation 1 (MyoD)* gene (Figure 4B). Besides, we demonstrated the contribution of cholesterol in NFATc1-driven GC resistance in T-ALL cells by combining exogenous cholesterol administration with dex treatment. Specifically, the exogenous cholesterol restores GC resistance exclusively in *NFATc1* knock-down cells comparable to intrinsically resistant control cells' levels (Figure 4C). Conversely, the inhibition of cholesterol biosynthesis by simvastatin both *in vitro* or *in vivo* strongly synergizes with dex in reducing GC resistant T-ALL cells' proliferation and viability by restoring the canonical GR transcriptional activity (Figure 4D-E and S8D-E, S9A). Altogether these results indicate that NFATc1 contributes to T-ALL GC resistance by directly regulating key enzymes involved in cholesterol biosynthesis, whose inhibition increases GC sensitivity by restoring the GR ability to transcribe primary target genes.

Cholesterol contributes to NFATc1-driven GC resistance by sustaining the formation of plasma membrane LRs and the activation of LCK and PLCγ proteins

Subsequently, we inquired deeper on how cholesterol participates in NFATc1-driven GC resistance in T-ALL cells. Starting from the evidence that in NFATc1 absence, the two main components of LRs [29], cholesterol and sphingolipids, are significantly reduced (Figure S8B), we quantified the abundance of LRs in *NFATc1* knock-down cells. Interestingly, we detected a significant decrease in LRs number, together with a reduced expression of the anchored CD4 co-receptor and the LCK kinase in ALL-SIL and TALL-1 cell lines after *NFATc1* gene silencing (Figures 5A-C, S9B). Moreover, in the same cell lines, we observed a reduction of LCK active form (SRC Y416) as well as of the activation of the LCK downstream Phospholipase C Gamma active form (PLCγ Y783) (Figure 5D, top panel). Consistently with this evidence, the ectopic *NFATc1* expression in the 720 and 5146 T-ALL cell lines led mostly to an increase in LCK protein activation (SRC Y416) (Figure 5D, bottom panel) suggesting a possible regulation of the entire TCR/LCK signaling cascade mediated by NFATc1 in T-ALL cells. Finally, we also observed a decrease in the expression and activation of LCK, PLCγ Y783 and NFATc1 itself after simvastatin treatment (Figure S9C). Thus, given the well-known role of LCK kinase signaling in supporting GC resistance [8-11], our data indicates that a possible mechanism by which NFATc1 guides T-ALL GC resistance is by sustaining the TCR/LCK entirely signaling cascade playing on the intracellular cholesterol levels and LRs abundance.

NFATc2 influences GC resistant T-ALL cells' differentiation and confers resistance to GC treatment through direct regulation of the WNT/β-catenin pathway

To assess the putative molecular processes involved in GC response driven by NFATc2, we performed transcriptome analysis on RPMI-8402 *NFATc2* knock-down cells and relative controls. Interestingly, among the most significantly upregulated BPs we found the T-cell pro-differentiation (Figure S10). In agreement, among the surface markers routinely used in the diagnostic procedure, we observed a reduced percentage of $CD34^+$ T-ALL cells and an increase of $CD7^+$ one after *NFATc2* gene silencing compared to controls (Figure 6A and S11A). This result is consistent with the reduced/increased levels of *CD34/CD7* mRNA, detected by GEP analysis (Figure S11B). Of note, no changes on *CD34* and *CD7* expressions were observed in TALL-1 ShRNA *NFATc1* compared to control, further suggesting that the two NFATs regulate different cellular processes (Figures S11C-D). In a complementary manner, we observed the WNT/β-Catenin signaling pathway, which is a well-known process to be involved in cancer stem cell maintenance and chemotherapy resistance [30,31], among the most significantly downregulated biological processes in absence of *NFATc2* (Figure S12A). Using immunoblotting, we confirmed that *NFATc2* silencing markedly reduced the expression of proteins belonging to WNT/β-Catenin signaling, such as the β-Catenin, the *LDL Receptor Related Protein 6* (LRP6), the *Transcription Factor 7 Like 2* (TCF-4) and the *Hematopoietically Expressed Homeobox* (HHEX) in RPMI-8402 and LOUCY cell lines (Figure 6B). Additionally, to assess if NFATc2 exerted a direct regulation on WNT/β-Catenin signaling pathway, we performed ChIP experiments for NFATc2 protein on RPMI-8402 cell line. Interestingly, we revealed a significant enrichment of NFATc2 DNA binding sequence in the *LRP6* promoter. Of note, no positive enrichment has been observed for the IgG and *MyoD* gene, thus suggesting that NFATc2 directly regulates *LRP6* expression (Figure 6C). Besides this, we demonstrated that the WNT/β-Catenin pathway participates in NFATc2-driven GC resistance in T-ALL cells. Indeed, the addition of exogenous WNT3a ligand restores the intrinsic GC resistance of control cells in RPMI-8402 and LOUCY ShRNA *NFATc2* expressing cells treated with dex (Figure 6D). Consistently with these findings, the WNT/β-Catenin inhibitor PRI-724 [32] strongly synergizes with dex on reducing RPMI-8402 as well as LOUCY GC resistant cells' proliferation and viability by restoring GR transcriptional activity (Figures 6E-F, S12B-C). Overall, these data suggest that NFATc2 can affect T-ALL cells' differentiation and contributes to GC resistance by directly modulating WNT/β-Catenin signaling.

Finally, we observed that among the PPR patients (n=12), the ones with a high MRD count at day +78 ($>10^{-3}$) are characterized by a significant enrichment of genes related to WNT signaling pathway. On the contrary, the PPR patients (n=16) with a low MRD value ($< 10^{-3}$) show an enrichment of genes belonging to cholesterol homeostasis (Figure S13). The association of distinct biological processes with different MRD levels suggests their potential not only as novel therapeutic targets but also as new prognostic markers for PPR patients.

Discussion

Glucocorticoid resistance represents a major hurdle in the treatment of approximately 20-25% of T-ALL pediatric patients, for whom the prognosis remains quite poor [5-7]. Despite extensive research highlighting several oncogenic pathways that impair GR functions, such as AKT-mediated phosphorylation preventing GR nuclear translocation [33], or aberrant activation of the IL7R pathway [34], the molecular mechanisms underlying GC resistance remain poorly understood. In this study, we present the first evidence of the involvement of NFATc1 and NFATc2 in GC resistance, identifying them as novel potential therapeutic targets in T-ALL.

We discovered that PPR patients, at diagnosis, display elevated levels of NFATc1 and NFATc2, along with reduced GR transcriptional activity. In contrast, PGR patients exhibit much more robust GR signaling and activity than NFATc1 and NFATc2. These findings suggest that PPR patients are characterized by an impaired GR transcriptional function already at diagnosis, rather by an intrinsic low *NR3C1* mRNA expression, as previously reported in T-ALL patients at relapse [35]. It is very important to mention here that *NR3C1* genetic aberrations are rare at diagnosis [36,37], therefore our findings suggest that reduced GR transcriptional activity may be caused by non-genetic factors [4,38], such as the dysregulation of NFATc1 and NFATc2. The synergistic effect of CsA and dexamethasone on cell proliferation and viability of primary and T-ALL cell lines, highlights the crucial role of NFAT transcription factors in GC resistance. Accordingly, we found that specific gene silencing of *NFATc1* or *NFATc2* in GC-resistant T-ALL cells restored GR activity, thereby sensitizing the cells to dexamethasone therapy both *in vitro* and *vivo*. Indeed, reactivation of GR's function assessed by the increased GR luciferase activity upon *NFATc1* or *c2* silencing, led to the expression of *BCL2L11* in the presence of dexamethasone, in agreement to previous reports [39-41], supporting our findings of a negative correlation between NFATc1/c2 activity and GR function in primary T-ALL patient samples. Notably, despite the known role of ABCB1 drug transporter in managing GC efflux [21-23,42,43], we observed no changes in its expression or activity during the restoration of GC sensitivity, reinforcing the idea that NFATc1 and NFATc2 are central players in GC resistance.

From a wide analysis of BPs affected by *NFATc1* gene silencing we observed a significant downregulation of MYC target genes as well as of genes primarily involved in cell cycle regulation and cholesterol biosynthesis. However, while NFATc1's role to promote cell cycle progression by modulating cyclin expression is well-known and perfectly aligns with our findings [24,25], its regulation of cholesterol biosynthesis is an entirely new discovery. Interestingly, in recent years a large body of evidence on the critical role of cholesterol metabolism in cancer development and resistance to treatment is emerging [26-28]. Particularly, in childhood ALL the upregulation of cholesterol biosynthetic pathway was reported to support central nervous system invasion [44]. Moreover, this mechanism contributes to the poor prognosis of the high risk ETP-ALL patient subgroup through regulation of AKT1/MYC signaling axis [26]. Given these compelling associations, we focused on cholesterol biosynthesis to dissect its relationship with NFATc1 and T-ALL GC resistance. Our study reveals that NFATc1 directly regulates key enzymes of cholesterol biosynthesis, thereby maintaining the lipid rafts' formation, where the CD4 co-receptor and the TCR are anchored, thus allowing the activation of the LCK signaling cascade [45,46]. Given the link shown by our group between LCK hyperactivation and GC resistance [8], mechanistically, we propose a positive feedback loop between NFATc1 and LCK to drive T-ALL GC resistance. Moreover, our results are in good agreement with previous findings that cholesterol-enriched LRs maintain NFATc1 activation, and that inhibiting the mevalonate pathway (e.g., with simvastatin) restores GC response both *in vitro* and *in vivo* [47-49], further supporting the critical role of cholesterol in NFATc1-driven GC resistance. In line, overexpressing *NFATc1* in GC-sensitive cells or supplementing cholesterol in *NFATc1*-depleted T-ALL cells both induce dexamethasone resistance. This makes the cholesterol biosynthesis pathway a critical focus for future research aimed at overcoming GC resistance in leukemia.

Furthermore, our finding that *NFATc2* silencing in T-ALL GC-resistant cells enhance T-cell differentiation and downregulates the key regulator of T-cell stemness WNT/β-catenin pathway is also extremely novel as this pathway is hyperactivated in around 80% of pediatric T-ALL cases [50]. Thus, we demonstrated that NFATc2 directly binds the LRP6 promoter, positively regulating WNT/β-catenin signaling and supporting GC resistance. Indeed, the WNT/β-catenin induction signaling in *NFATc2*-depleted T-ALL cells also restore resistance to GC treatment, similarly to the overexpression of

NFATc2 in GC sensitive cell lines. As a result, the pharmacological inhibition of WNT/β-catenin signaling with PRI-724 restored GC sensitivity by reactivating GR function, in accordance with what previously shown in B-ALL cells [51]. Lastly, while NFAT proteins are known to regulate T-cell differentiation [52], for the first time our work establishes a direct connection between NFATc2 depletion and WNT/β-catenin downregulation as well as changes in *CD34* and *CD7* expression in T-ALL cells. Most importantly, considering that $CD34^+$ is a leukemia initiating cells (LICs) marker [53], we can here speculate that *NFATc2* depletion reduces the rate of LICs responsible for therapy resistance and relapse, as already described for high MRD patients [5], although further *vivo* experiments are necessary to assess it.

In conclusion, our discovery that NFATc1 and NFATc2 control two distinct and independent biological processes marks a pivotal breakthrough in understanding the molecular mechanisms behind GC resistance in pediatric T-ALL. For the first time, we have shown both *in vitro* and *in vivo* that these transcription factors play a central role in regulating T-ALL cells' response to glucocorticoids, with NFATc1 driving cholesterol biosynthesis and NFATc2 governing WNT/β-catenin signaling. What makes this finding particularly exciting is the way these pathways correlate with MRD levels at day +78 in PPR patients. Indeed, we observed that cholesterol pathway homeostasis was associated with low MRD levels, while WNT/β-catenin signaling related to higher MRD. These distinct associations not only reinforce the NFATc1 and NFATc2 crucial roles in GC resistance but also suggest that these pathways serve as valuable prognostic markers for PPR patients as well as putative novel therapeutic targets. In this context, however, current treatments targeting the Calcineurin/NFAT pathway, such as CsA and FK506, are limited by non-specific off-targets and significant side effects [14,15,54,55]. Other approaches, like inhibiting the upstream LCK kinase with dasatinib in PPR patients [8-11], are so far effective only in a subset of T-ALL patients [56]. Simvastatin and PRI-724 have shown limited applicability in the pediatric population due to concerns related to developmental toxicity and a lack of significant clinical efficacy [57], as reported in trials NCT01302405 and NCT03620474. Nevertheless, in the adult group statins seem to have been associated with a protective effect against leukemogenesis and with improved molecular response in Chronic Myeloid Leukemia [58-59]. Therefore, the design of novel specific NFATc1 and NFATc2 inhibitors is crucial to overcome the limitations of current therapies and improve treatment options for T-ALL patients, offering a promising path forward for more targeted and effective treatments.

Reference

[1] Van Vlierberghe P, Ferrando A. The molecular basis of T cell acute lymphoblastic leukemia. J Clin Invest. 2012;122(10):3398-3406.

[2] Inaba H, Pui CH. Glucocorticoid use in acute lymphoblastic leukaemia. Lancet Oncol. 2010;11(11):1096-1106.

[3] Löwenberg M, Verhaar AP, Bilderbeek J, et al. Glucocorticoids cause rapid dissociation of a T-cell-receptor-associated protein complex containing LCK and FYN. EMBO Rep. 2006;7(10):1023-1029.

[4] Borin C, Pieters T, Serafin V, Ntziachristos P. Emerging Epigenetic and Posttranslational Mechanisms Controlling Resistance to Glucocorticoids in Acute Lymphoblastic Leukemia. Hemasphere. 2023;7(7):e916.

[5] Schrappe M, Valsecchi MG, Bartram CR, et al. Late MRD response determines relapse risk overall and in subsets of childhood T-cell ALL: results of the AIEOP-BFM-ALL 2000 study. Blood. 2011;118(8):2077-2084.

[6] Cario G, Valsecchi MG, Conter V, et al. Results in Pediatric T-ALL Patients Treated in Trial AIEOP-BFM ALL 2009: Exploring Prognostic Factors in the Context of Modern Risk Adapted Therapy. Blood. 2024;144(2024):730-731.

[7] Buchmann S, Schrappe M, Baruchel A, et al. Remission, treatment failure, and relapse in pediatric ALL: an international consensus of the Ponte-di-Legno Consortium. Blood. 2022;139(12):1785-1793.

[8] Serafin V, Capuzzo G, Milani G, et al. Glucocorticoid resistance is reverted by LCK inhibition in pediatric T-cell acute lymphoblastic leukemia. Blood. 2017;130(25):2750-2761.

[9] Serafin V, Lissandron V, Buldini B, et al. Phosphoproteomic analysis reveals hyperactivation of mTOR/STAT3 and LCK/Calcineurin axes in pediatric early T-cell precursor ALL. Leukemia. 2017;31(4):1007-1011.

[10] Shi Y, Beckett MC, Blair HJ, et al. Phase II-like murine trial identifies synergy between dexamethasone and dasatinib in T-cell acute lymphoblastic leukemia. Haematologica. 2021;106(4):1056-1066.

[11] Fazio G, Bresolin S, Silvestri D, et al. PAX5 fusion genes are frequent in poor risk childhood acute lymphoblastic leukaemia and can be targeted with BIBF1120. EBioMedicine. 2022;83:104224.

[12] Mancini M, Toker A. NFAT proteins: emerging roles in cancer progression. Nat Rev Cancer. 2009;9(11):810-820.

[13] Macian F. NFAT proteins: key regulators of T-cell development and function. Nat Rev Immunol. 2005;5(6):472-484.

[14] Bucher P, Erdmann T, Grondona P, et al. Targeting chronic NFAT activation with calcineurin inhibitors in diffuse large B-cell lymphoma. Blood. 2020;135(2):121-132.

[15] Medyouf H, Alcalde H, Berthier C, et al. Targeting calcineurin activation as a therapeutic strategy for T-cell acute lymphoblastic leukemia. Nat Med. 2007;13(6):736-741.

[16] Bond J, Tran Quang C, Hypolite G, et al. Novel Intergenically Spliced Chimera, NFATC3-PLA2G15, Is Associated with Aggressive T-ALL Biology and Outcome. Mol Cancer Res. 2018;16(3):470-475.

[17] Catherinet C, Passaro D, Gachet S, et al. NFAT transcription factors are essential and redundant actors for leukemia initiating potential in T-cell acute lymphoblastic leukemia. PLoS One. 2021;16(7):e0254184.

[18] Haferlach T, Kohlmann A, Wieczorek L, et al. Clinical utility of microarray-based gene expression profiling in the diagnosis and subclassification of leukemia: report from the International Microarray Innovations in Leukemia Study Group. J Clin Oncol. 2010;28(15):2529-2537.

[19] Pinazza M, Borga C, Agnusdei V, et al. An immediate transcriptional signature associated with response to the histone deacetylase inhibitor Givinostat in T acute lymphoblastic leukemia xenografts. Cell Death Dis. 2016;6(1):e2047.
[20] Dong X, Ding L, Thrasher A, et al. NetBID2 provides comprehensive hidden driver analysis. Nat Commun. 2023;14(1):2581.
[21] Ueda K, Okamura N, Hirai M, et al. P-glycoprotein transports cortisol, aldosterone, and dexamethasone, but not progesterone. J Biol Chem. 1992;267(34):24248-24252.
[22] Bourgeois S, Gruol DJ, Newby RF, et al. Expression of an mdr gene is associated with a new form of resistance to dexamethasone-induced apoptosis. Mol Endocrinol. 1993;7(7):840-8 51.
[23] Devine K, Villalobos E, Kyle CJ, et al. The ATP-binding cassette proteins ABCB1 and ABCC1 as modulators of glucocorticoid action. Nat Rev Endocrinol. 2023;19(2):112-124.
[24] Medyouf H, Ghysdael J. The calcineurin/NFAT signaling pathway: a novel therapeutic target in leukemia and solid tumors. Cell Cycle. 2008;7(3):297-303.
[25] Mognol GP, Carneiro FR, Robbs BK, Faget DV, Viola JP. Cell cycle and apoptosis regulation by NFAT transcription factors: new roles for an old player. Cell Death Dis. 2016;7(4):e2199.
[26] Rashkovan M, Albero R, Gianni F, et al. Intracellular Cholesterol Pools Regulate Oncogenic Signaling and Epigenetic Circuitries in Early T-cell Precursor Acute Lymphoblastic Leukemia. Cancer Discov. 2022;12(3):856-871.
[27] Chen YY, Ge JY, Zhu SY, et al. Copy number amplification of ENSA promotes the progression of triple-negative breast cancer via cholesterol biosynthesis. Nat Commun. 2022;13(1):791.
[28] Mok EHK, Leung CON, Zhou L, et al. Caspase-3-Induced Activation of SREBP2 Drives Drug Resistance via Promotion of Cholesterol Biosynthesis in Hepatocellular Carcinoma. Cancer Res. 2022;82(17):3102-3115.
[29] Lingwood D, Simons K. Lipid rafts as a membrane-organizing principle. Science. 2010;327(5961):46-50.
[30] Parsons MJ, Tammela T, Dow LE. WNT as a Driver and Dependency in Cancer. Cancer Discov. 2021;11(10):2413-2429.
[31] Reya T, Clevers H. Wnt signalling in stem cells and cancer. Nature. 2005;434(7035):843-850.
[32] El-Khoueiry AB, Ning Y, Yang D, et al. A phase I first-in-human study of PRI-724 in patients (pts) with advanced solid tumors. J Clin Oncol. 2013;31(15_suppl):2501.
[33] Piovan E, Yu J, Tosello V, Herranz D, et al. Direct reversal of glucocorticoid resistance by AKT inhibition in acute lymphoblastic leukemia. Cancer Cell. 2013;24(6):766-776.
[34] Li Y, Buijs-Gladdines JG, Canté-Barrett K, et al. IL-7 Receptor Mutations and Steroid Resistance in Pediatric T cell Acute Lymphoblastic Leukemia: A Genome Sequencing Study. PLoS Med. 2016;13(12):e1002200.
[35] Wandler AM, Huang BJ, Craig JW, et al. Loss of glucocorticoid receptor expression mediates in vivo dexamethasone resistance in T-cell acute lymphoblastic leukemia. Leukemia. 2020;34(8):2025-2037.
[36] Liu H, Li Z, Qiu F, et al. Association Between NR3C1 Mutations and glucocorticoid resistance in children with acute lymphoblastic leukemia. Front Pharmacol. 2021;12:634956.
[37] Van der Zwet JCG, Smits W, Buijs-Gladdines JGCAM, Pieters R, Meijerink JPP. Recurrent NR3C1 Aberrations at First Diagnosis Relate to Steroid Resistance in Pediatric T-Cell Acute Lymphoblastic Leukemia Patients. Hemasphere. 2020;5(1):e513.
[38] Jin Q, Gutierrez Diaz B, Pieters T, et al. Oncogenic deubiquitination controls tyrosine kinase signaling and therapy response in acute lymphoblastic leukemia. Sci Adv. 2022;9;8(49):eabq8437.
[39] Toscan CE, Jing D, Mayoh C, Lock RB. Reversal of glucocorticoid resistance in paediatric acute lymphoblastic leukaemia is dependent on restoring BIM expression. Br J Cancer. 2020;122(12):1769-1781.

[40] Brown JA, Ferrando A. Glucocorticoid Resistance in Acute Lymphoblastic Leukemia: BIM Finally. Cancer Cell. 2018;34(6):869-871.
[41] Veltri G, Silvestri C, Gallingani I, et al. Ruxolitinib as a Novel Therapeutic Option for Poor Prognosis T-LBL Pediatric Patients. Cancers (Basel). 2021;13(15):3724.
[42] Aberuyi N, Rahgozar S, Pourabutaleb E, Ghaedi K. Selective dysregulation of ABC transporters in methotrexate-resistant leukemia T-cells can confer cross-resistance to cytarabine, vincristine and dexamethasone, but not doxorubicin. Curr Res Transl Med. 2021;69(1):103269.
[43] Peng R, Zhang H, Zhang Y, Wei DY. Impacts of ABCB1 (G1199A) polymorphism on resistance, uptake, and efflux to steroid drugs. Xenobiotica. 2016;46(10):948-952.
[44] Cousins A, Olivares O, Markert E, et al. Central nervous system involvement in childhood acute lymphoblastic leukemia is linked to upregulation of cholesterol biosynthetic pathways. Leukemia. 2022;36(12):2903-2907.
[45] Ballek O, Broučková A, Manning J, Filipp D. A specific type of membrane microdomains is involved in the maintenance and translocation of kinase active Lck to lipid rafts. Immunol Lett. 2012;142(1-2):64-74.
[46] Viola A, Schroeder S, Sakakibara Y, Lanzavecchia A. T lymphocyte costimulation mediated by reorganization of membrane microdomains. Science. 1999;283(5402):680-682.
[47] Levin-Gromiko U, Koshelev V, Kushnir P, Fedida-Metula S, Voronov E, Fishman D. Amplified lipid rafts of malignant cells constitute a target for inhibition of aberrantly active NFAT and melanoma tumor growth by the aminobisphosphonate zoledronic acid. Carcinogenesis. 2014;35(11):2555-2566.
[48] Beesley AH, Firth MJ, Ford J, et al. Glucocorticoid resistance in T-lineage acute lymphoblastic leukaemia is associated with a proliferative metabolism. Br J Cancer. 2009;100(12):1926-1936.
[49] Samuels AL, Heng JY, Beesley AH, Kees UR. Bioenergetic modulation overcomes glucocorticoid resistance in T-lineage acute lymphoblastic leukaemia. Br J Haematol. 2014;165(1):57-66.
[50] Chiarini F, Paganelli F, Martelli AM, Evangelisti C. The Role Played by Wnt/β-Catenin Signaling Pathway in Acute Lymphoblastic Leukemia. Int J Mol Sci. 2020;21(3):1098.
[51] Gang EJ, Hsieh YT, Pham J, et al. Small-molecule inhibition of CBP/catenin interactions eliminates drug-resistant clones in acute lymphoblastic leukemia. Oncogene. 2014;33(17):2169-2178.
[52] Peng SL, Gerth AJ, Ranger AM, Glimcher LH. NFATc1 and NFATc2 together control both T and B cell activation and differentiation. Immunity. 2001;14(1):13-20.
[53] Gerby B, Clappier E, Armstrong F, et al. Expression of CD34 and CD7 on human T-cell acute lymphoblastic leukemia discriminates functionally heterogeneous cell populations. Leukemia. 2011;25(8):1249-1258.
[54] Müller MR, Rao A. Linking calcineurin activity to leukemogenesis. Nat Med. 2007;13(6):669-671.
[55] Müller MR, Rao A. NFAT, immunity and cancer: a transcription factor comes of age. Nat Rev Immunol. 2010;10(9):645-656.
[56] Cerchione C, Locatelli F, Martinelli G. Dasatinib in the management of pediatric patients with philadelphia chromosome-positive acute lymphoblastic leukemia. Front Oncol. 2021;11:632231.
[57] Fiorentino R, Chiarelli F. Statins in Children, an Update. Int J Mol Sci. 2023;24(2):1366.
[58] Pradelli D, Soranna D, Zambon A, et al. Statins use and the risk of all and subtype hematological malignancies: a meta-analysis of observational studies. Cancer Med. 2015;4(5):770-780.
[59] Jang H-J, Woo Y-M, Naka K, et al. Statins Enhance the Molecular Response in Chronic Myeloid Leukemia when Combined with Tyrosine Kinase Inhibitors. Cancers (Basel). 2021;13(21):5543.

Figure legends

Figure 1: NFATc1 and NFATc2 guide GC resistance in T-ALL. (A) Volcano plot of NetBid2 inferred transcription factor (TF) and signaling (SIG) activity in PGR versus PPR patients. In x-axis log2 fold change; in y-axis the p-value. (B) Heatmap showing Pearson's correlation values between *NFATc1, NFATc2* and *NR3C1* activity in 104 T-ALL pediatric patients at the diagnosis. (C) Heatmap and hierarchical clustering analysis of *NFATc1*, *NFATc2* and *NR3C1* transcriptional activity and signaling in T-ALL pediatric patients at diagnosis; color annotations are based on GC response (upper bar) and T-ALL patients molecular subtypes (lower bar). (D) 2D matrix representing Bliss synergy score of CsA and dex in reducing ALL-SIL, RPMI-8402, TALL-1 and LOUCY GC resistant cells and (E) *ex vivo* primary T-ALL GC resistant cells' proliferation after 72 hours of treatment.

Figure 2: *NFATc1* or *NFATc2* knock-down sensitizes T-ALL cells to dex treatment *in vivo* zebrafish model. Lateral view of the trunk region of Tg(Fli1:GFP) embryos injected with with approximately 200 pre-labelled DiL^+ (A) TALL-1 ShRNA *CNTR* and ShRNA *NFATc1* and (B) RPMI-8402 ShRNA *CNTR* and ShRNA *NFATc2* (orange) cells, after 24 hours of treatment with dex 10 µM or DMSO (control group). On the right, quantification of the orange intensity signal associated with transplanted cells. Scale bar, 100 µm. Results are presented as means + SEM (unpaired t- test;* $p < 0.05$; *** $p < 0.001$), $n \geq 3$ for all the experiments. (C) Percentage of live primary T-ALL cells transiently silenced for NFATc1 or NFATc2 gene expression after 48 hours of *ex vivo* dex treatment (1 µM). Primary cells are derived from PDXs grafted with GC-resistant T-ALL patients (n=4). Results are presented as means + SEM (paired t-test; * $p < 0.05$; *** $p < 0.001$, **** $p < 0.0001$), $n \geq 3$ for all the experiments.

Figure 3: *NFATc1* or *NFATc2* knock-down sensitizes T-ALL cells to dex treatment by restoring the GR transcriptional activity (A) GSEA for GO-BP response to corticosteroid gene set in TALL-1 *NFATc1* and RPMI-8402 *NFATc2* knock down cells treated with dex compared to control cells treated in the same conditions (normalized enrichment score (NES)=2.0 for TALL-1 and NES=1.89 for RPMI-8402, $p<0.001$). Venn diagram of genes upregulated by dex in (B) TALL-1 ShRNA *CNTR* or *NFATc1* and RPMI-8402 ShRNA *CNTR* or *NFATc2* and (C) TALL-1 ShRNA *NFATc1* and RPMI-8402 ShRNA *NFATc2* and P12-ICHIKAWA. Circled, the number of genes positively regulated by dex and in common between the groups. (D) GR transcriptional luciferase activity measured on ALL-SIL, TALL-1, RPMI-8402 and LOUCY cell lines stably silenced for *NFATc1* or *NFATc2* expression and controls, followed by the GR-GRE-luciferase plasmid reporter transfection and 6 hours of treatment with 10 µM dex. Results are presented as means + SEM (unpaired t-test;* $p < 0.05$), $n \geq 3$ for all the experiments.

Figure 4: NFATc1 confers GC resistance to T-ALL cells by directly modulating cholesterol biosynthesis, whose inhibition re-sensitizes T-ALL GC-resistant cells to dex treatment. (A) Intracellular unesterified cholesterol staining by Filipin III probe in ALL-SIL and TALL-1 *NFATc1* knock-down cells and controls. On the right side Filipin III median MFI absolute quantification. (B) ChIP analysis from TALL-1 cells. NFATc1 binding on the *DHCR7*, *HMGCS1*, *EBP* and *MyoD* promoters was compared with the IgG control. (C) Percentage of cell proliferation in ALL-SIL and TALL-1 *NFATc1* knock-down and control cells after 72 hours of treatment with exogenous cholesterol alone or in combination with dex. (D) 2D matrices displaying Bliss synergy score between simvastatin and dex in ALL-SIL and TALL-1 cells after 72 hours of treatment with scalar concentration of the two compounds. (E) *BCL2L11* and *TSC22D3* mRNA expression levels measured by RQ-PCR in ALL-SIL and TALL-1 cells pre-treated with 10 µM simvastatin for 4 hours followed by 5 µM and 1 µM of dex

respectively for 20 hours. Results are presented as means + SEM (paired t-test; * $p < 0.05$; ** $p < 0.01$; *** $p < 0.001$; **** $p < 0.0001$), $n \geq 3$ for all the experiments.

Figure 5: NFATc1-cholesterol driven GC resistance is mediated by plasma membrane LRs and LCK pathway activation. (A) On the left, fluorescent labeling of LRs in ALL-SIL and TALL-1 *NFATc1* knock down and control cells (scale bar represent 30 μm). On the right, relative quantification of the number of LRs per single cell. Results are presented as means + SEM (number of images analyzed n= 6 for each experiment. unpaired t-test; * $p < 0.05$; ** $p < 0.01$(B) Representative histogram showing percentage of $CD4^+$ cells in ALL-SIL and TALL-1 ShRNA *NFATc1* compared to control cells. (C) On the left, LCK staining in ALL-SIL and TALL-1 *NFATc1* knock-down cells and controls (scale bar represent 30 μm). On the right, the LCK MFI absolute quantification. Results are presented as means + SEM (unpaired t-test; * $p < 0.05$; ** $p < 0.01$) (D) WB analysis of NFATc1 or HA-NFATc1, SRC Y416, total LCK and PLCγ Y783 protein expression in ALL-SIL and TALL-1 *NFATc1* knock-down (upper part) or in 720 and 5146 *NFATc1* OE cells (lower part), and relative controls.

Figure 6: NFATc2 regulates T cell differentiation and WNT/β-catenin pathway, whose inhibition restores T-ALL GC resistant cells' response to dex administration. (A) Representative histogram showing the intensity expression of $CD34^+$ and $CD7^+$ cells in RPMI-8402 *NFATc2* knock-down and control cells. (B) WB analysis of NFATc2, LRP6, β-catenin, TCF-4, HHEX and GAPDH proteins' expression levels in RPMI-8402 and LOUCY *NFATc2* knock-down cells and controls. (C) ChIP analysis from RPMI-8402 cells. NFATc2 binding on the *LRP6* and *MyoD* promoters was compared with the IgG control. (D) Percentage of cell proliferation in RPMI-8402 and LOUCY *NFATc2* knock-down cells and the control cells after 72 hours of treatment with exogenous WNT3a ligand alone or in combination with dex. (E) 2D matrix representing Bliss synergy score of PRI-724 and dex in reducing RPMI-8402 and LOUCY cells' proliferation after 72 hours of treatment. (F) *BCL2L11* and *TSC22D3* mRNA expression levels measured by RQ-PCR in RPMI-8402 and LOUCY cells pre-treated with 2.5 μM PRI-724 for 4 hours followed by 1 μM dex for 20 hours. Results are presented as means + SEM (paired t test; * $p < 0.05$; ** $p < 0.01$; *** $p < 0.001$; **** $p < 0.0001$), $n \geq 3$ for all the experiments.

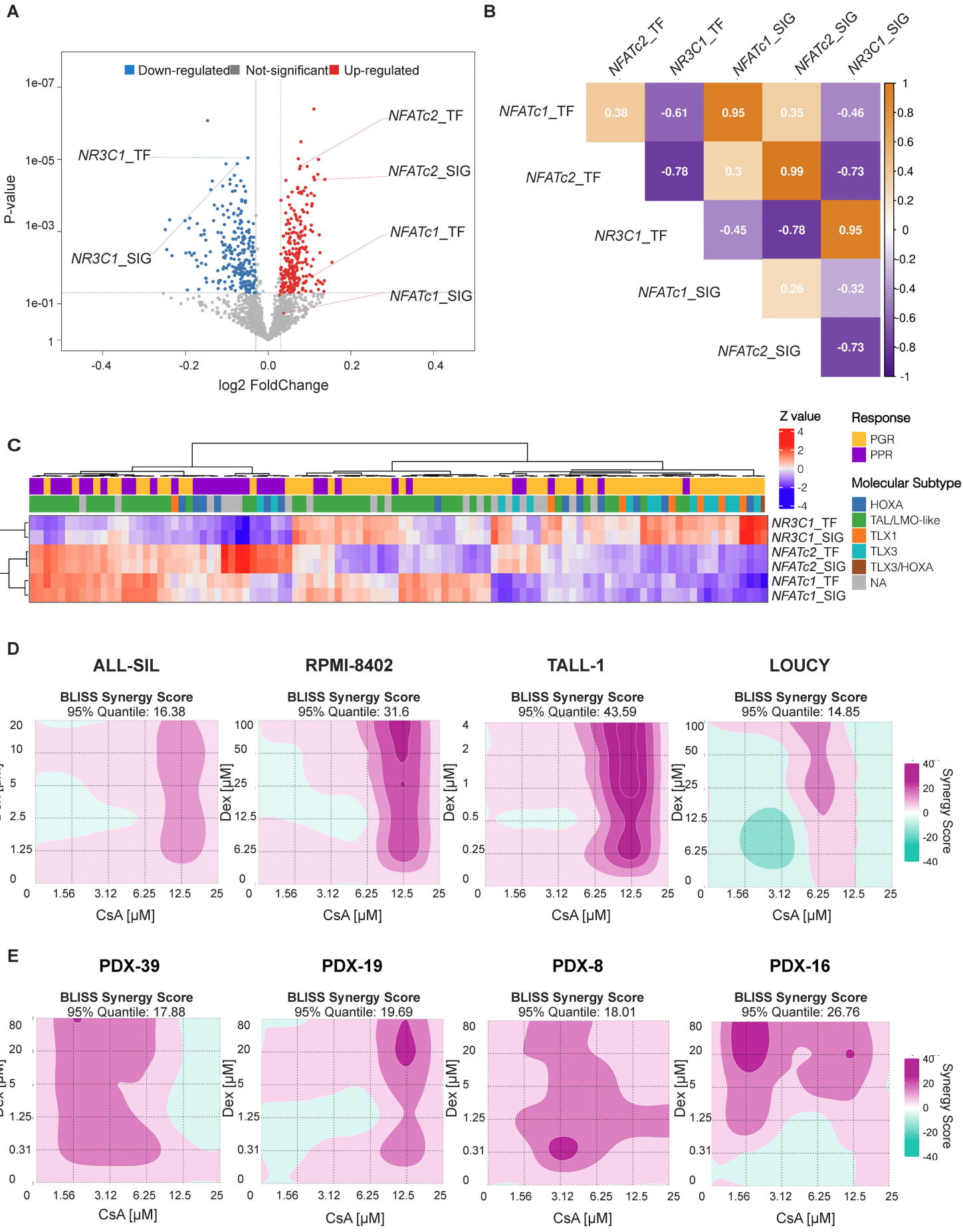
A
Down-regulated
Not-significant
Up-regulated
P-value
log2 FoldChange
NFATc2_TF
NR3C1_TF
NFATc2_SIG
NFATc1_TF
NR3C1_SIG
NFATc1_SIG
B
NFATc2_TF
NR3C1_TF
NFATc1_SIG
NFATc2_SIG
NR3C1_SIG
NFATc1_TF
0.38
-0.61
0.95
0.35
-0.46
-0.78
0.3
0.99
-0.73
-0.45
-0.78
0.95
0.26
-0.32
-0.73
C
Z value
Response
PGR
PPR
Molecular Subtype
HOXA
TAL/LMO-like
TLX1
TLX3
TLX3/HOXA
NA
D
ALL-SIL
RPMI-8402
TALL-1
LOUCY
BLISS Synergy Score
95% Quantile: 16.38
95% Quantile: 31.6
95% Quantile: 43.59
95% Quantile: 14.85
Dex [μM]
CsA [μM]
Synergy Score
E
PDX-39
PDX-19
PDX-8
PDX-16
95% Quantile: 17.88
95% Quantile: 19.69
95% Quantile: 18.01
95% Quantile: 26.76

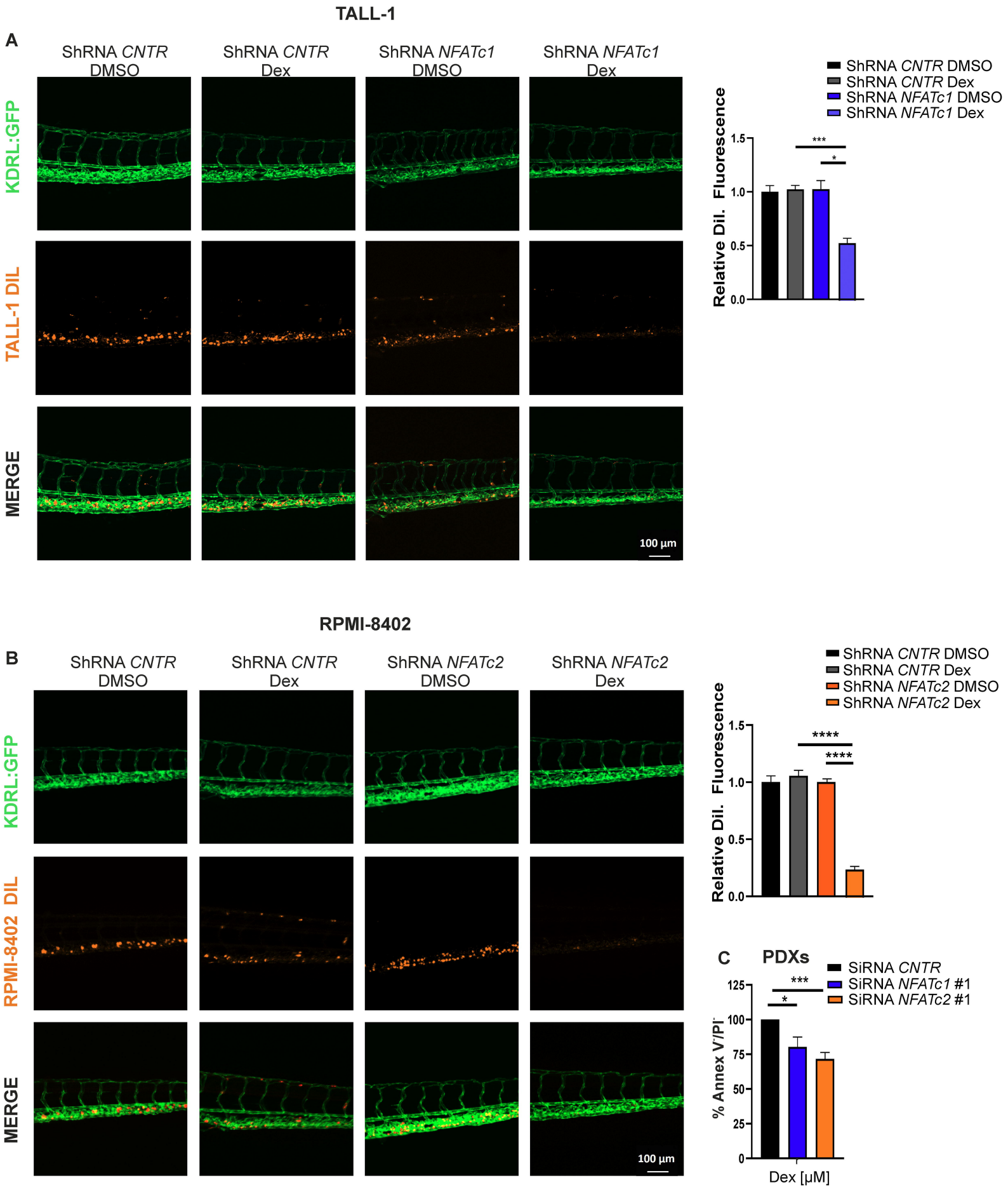
TALL-1
A
ShRNA CNTR DMSO
ShRNA CNTR Dex
ShRNA NFATc1 DMSO
ShRNA NFATc1 Dex
KDRL:GFP
TALL-1 DIL
MERGE
100 µm
ShRNA CNTR DMSO
ShRNA CNTR Dex
ShRNA NFATc1 DMSO
ShRNA NFATc1 Dex
Relative Dil. Fluorescence
1.5
1.0
0.5
0.0
***
*
RPMI-8402
B
ShRNA CNTR DMSO
ShRNA CNTR Dex
ShRNA NFATc2 DMSO
ShRNA NFATc2 Dex
KDRL:GFP
RPMI-8402 DIL
MERGE
100 µm
ShRNA CNTR DMSO
ShRNA CNTR Dex
ShRNA NFATc2 DMSO
ShRNA NFATc2 Dex
Relative Dil. Fluorescence
1.5
1.0
0.5
0.0
****
****
C
PDXs
SiRNA CNTR
SiRNA NFATc1 #1
SiRNA NFATc2 #1
% Annex V+/PI-
125
100
75
50
25
0
***
*
Dex [µM]

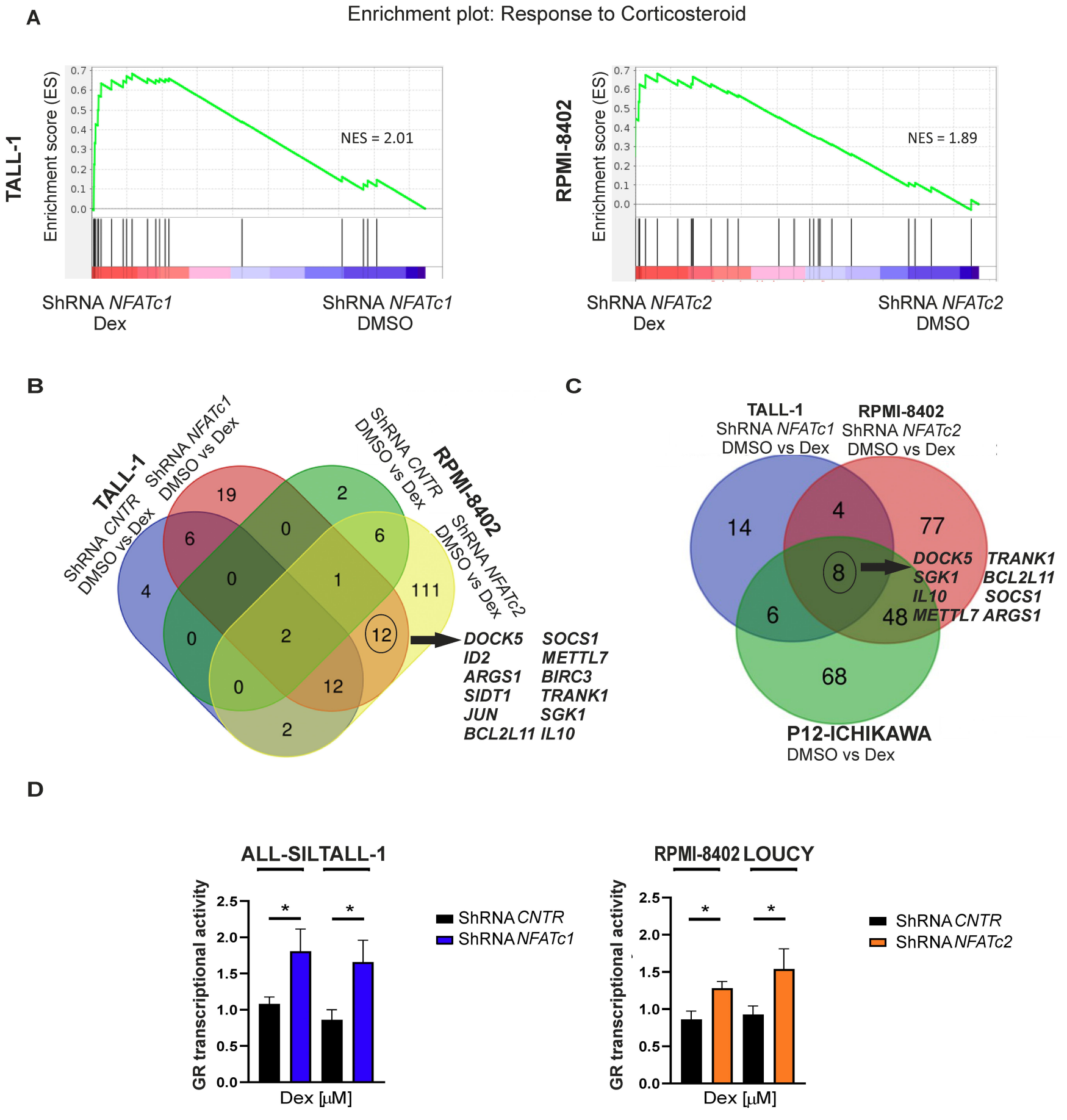
A
Enrichment plot: Response to Corticosteroid
TALL-1
Enrichment score (ES)
NES = 2.01
ShRNA NFATc1
Dex
ShRNA NFATc1
DMSO
RPMI-8402
Enrichment score (ES)
NES = 1.89
ShRNA NFATc2
Dex
ShRNA NFATc2
DMSO
B
TALL-1
ShRNA NFATc1
DMSO vs Dex
ShRNA CNTR
DMSO vs Dex
RPMI-8402
ShRNA CNTR
DMSO vs Dex
ShRNA NFATc2
DMSO vs Dex
19
2
6
0
6
4
0
1
111
0
2
12
0
12
2
DOCK5 SOCS1
ID2 METTL7
ARGS1 BIRC3
SIDT1 TRANK1
JUN SGK1
BCL2L11 IL10
C
TALL-1
ShRNA NFATc1
DMSO vs Dex
RPMI-8402
ShRNA NFATc2
DMSO vs Dex
14
4
77
8
DOCK5 TRANK1
SGK1 BCL2L11
IL10 SOCS1
6
48 METTL7 ARGS1
68
P12-ICHIKAWA
DMSO vs Dex
D
ALL-SILTALL-1
GR transcriptional activity
2.5
2.0
1.5
1.0
0.5
0.0
*
*
Dex [μM]
ShRNA CNTR
ShRNA NFATc1
RPMI-8402 LOUCY
GR transcriptional activity
2.5
2.0
1.5
1.0
0.5
0.0
*
*
Dex [μM]
ShRNA CNTR
ShRNA NFATc2

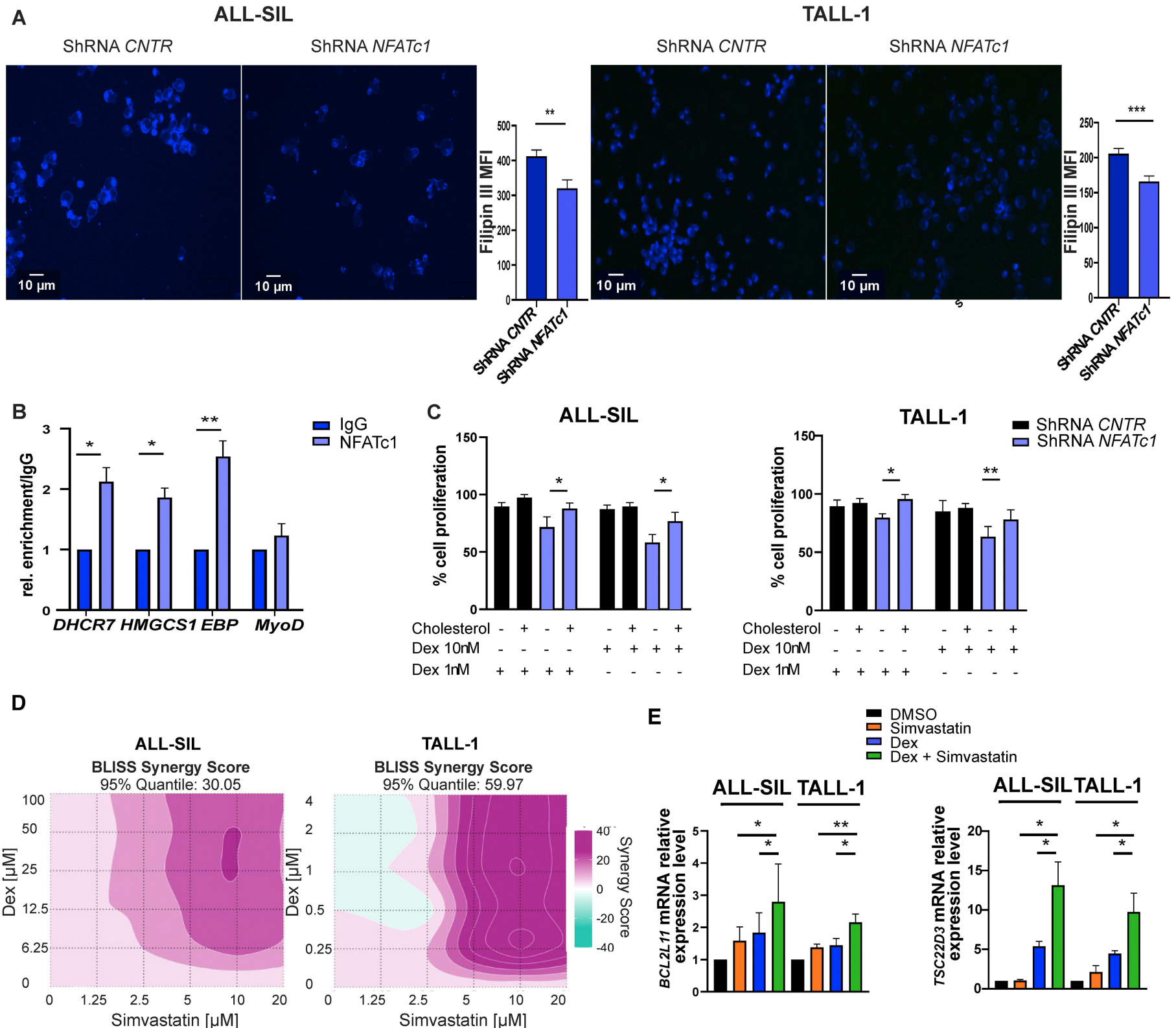
A
ALL-SIL
ShRNA CNTR
ShRNA NFATc1
10 µm
Filipin III MFI
**
ShRNA CNTR
ShRNA NFATc1
TALL-1
***
B
IgG
NFATc1
rel. enrichment/IgG
DHCR7
HMGCS1
EBP
MyoD
C
ALL-SIL
TALL-1
% cell proliferation
Cholesterol
Dex 10nM
Dex 1nM
D
BLISS Synergy Score
95% Quantile: 30.05
95% Quantile: 59.97
Dex [µM]
Simvastatin [µM]
Synergy Score
E
DMSO
Simvastatin
Dex
Dex + Simvastatin
BCL2L11 mRNA relative expression level
TSC22D3 mRNA relative expression level

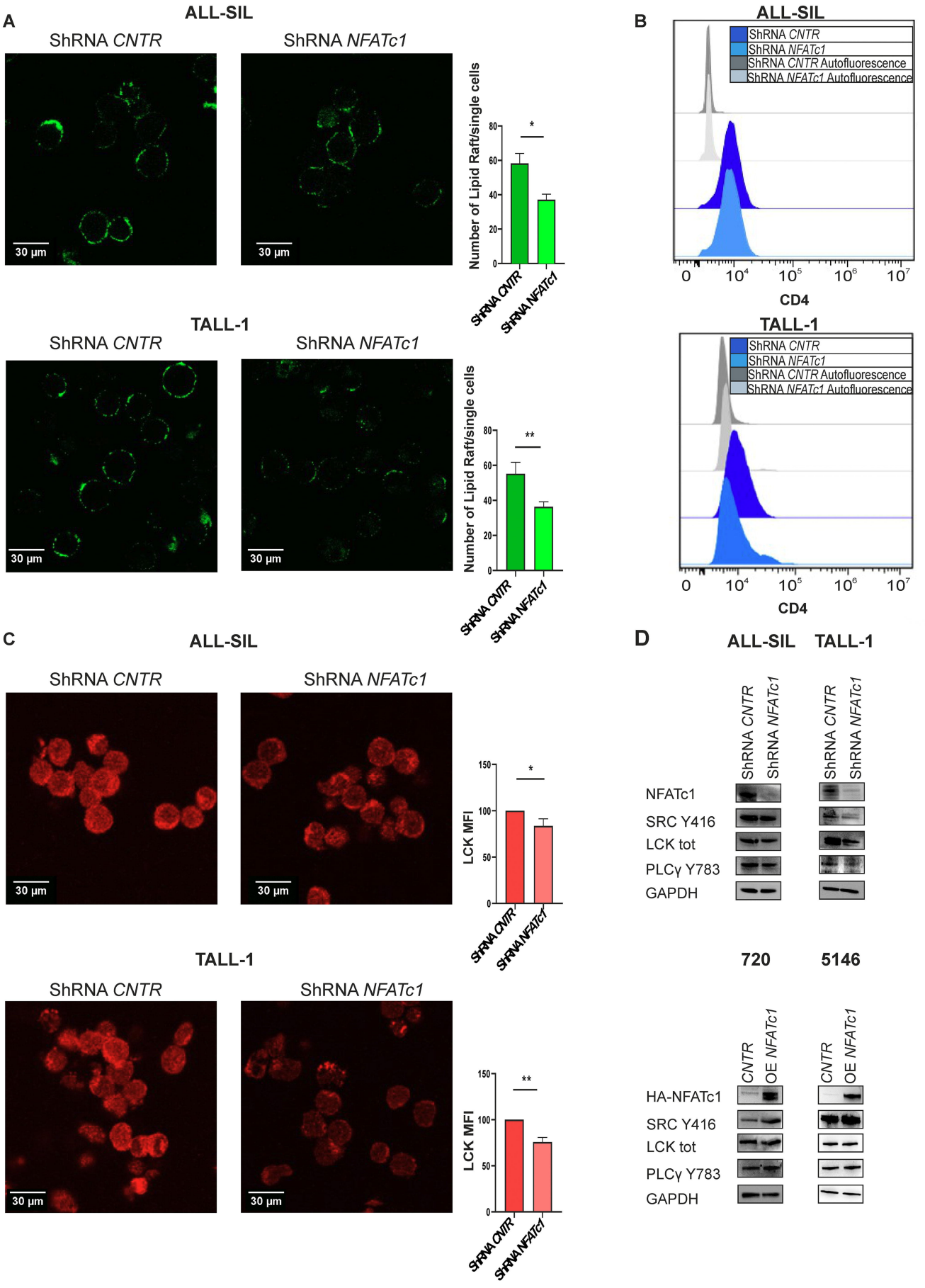
A
ALL-SIL
ShRNA CNTR
ShRNA NFATc1
30 µm
Number of Lipid Raft/single cells
ShRNA CNTR
ShRNA NFATc1
TALL-1
B
ALL-SIL
ShRNA CNTR
ShRNA NFATc1
ShRNA CNTR Autofluorescence
ShRNA NFATc1 Autofluorescence
CD4
TALL-1
C
LCK MFI
D
ALL-SIL
TALL-1
NFATc1
SRC Y416
LCK tot
PLCγ Y783
GAPDH
720
5146
CNTR
OE NFATc1
HA-NFATc1

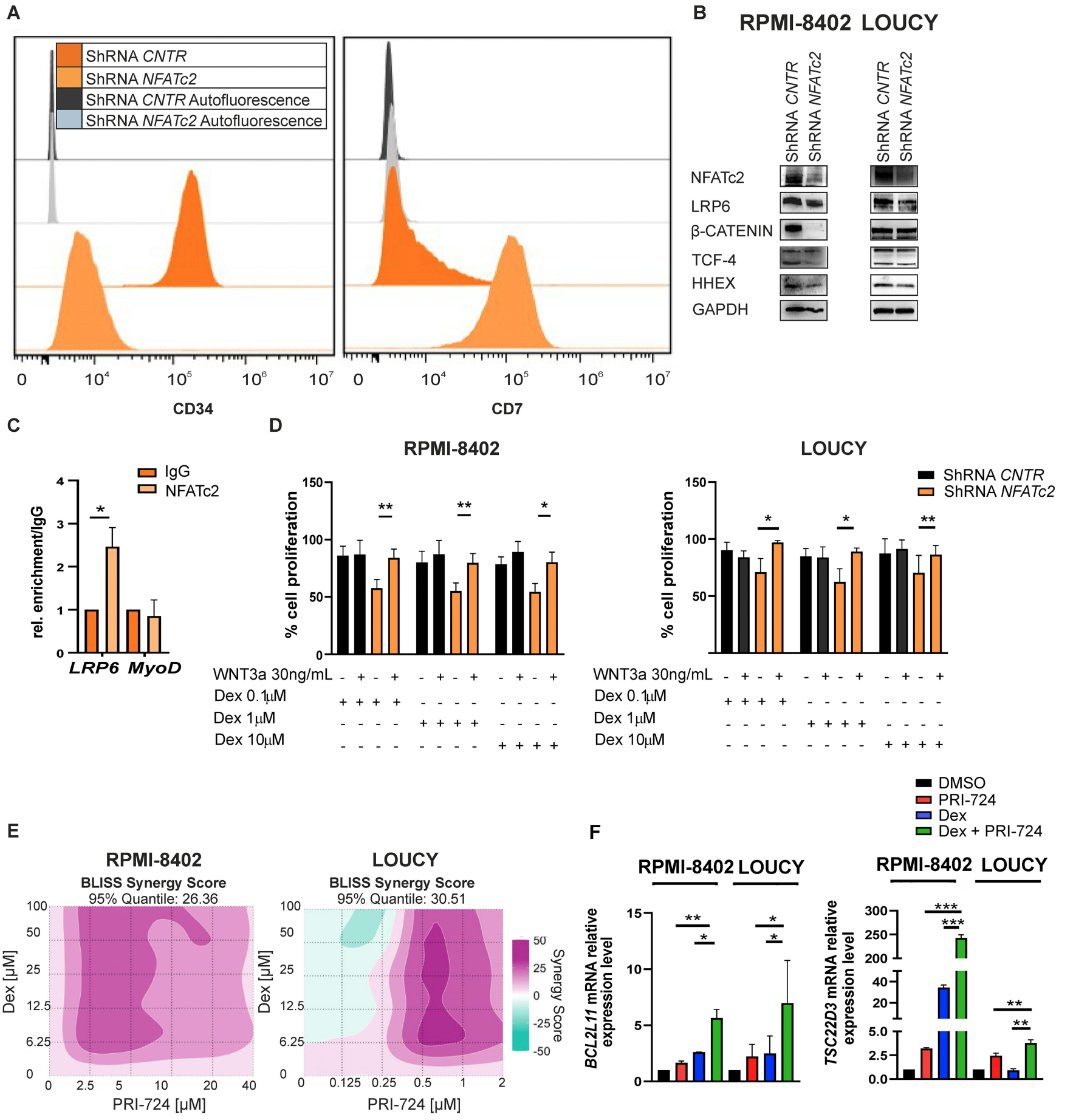
A
ShRNA CNTR
ShRNA NFATc2
ShRNA CNTR Autofluorescence
ShRNA NFATc2 Autofluorescence
CD34
CD7
B
RPMI-8402 LOUCY
ShRNA CNTR
ShRNA NFATc2
NFATc2
LRP6
β-CATENIN
TCF-4
HHEX
GAPDH
C
IgG
NFATc2
rel. enrichment/IgG
LRP6 MyoD
D
RPMI-8402
LOUCY
% cell proliferation
WNT3a 30ng/mL
Dex 0.1μM
Dex 1μM
Dex 10μM
E
RPMI-8402
LOUCY
BLISS Synergy Score
95% Quantile: 26.36
95% Quantile: 30.51
Dex [μM]
PRI-724 [μM]
Synergy Score
F
DMSO
PRI-724
Dex
Dex + PRI-724
RPMI-8402 LOUCY
BCL2L11 mRNA relative expression level
TSC22D3 mRNA relative expression level

NFATc1 and NFATc2 regulate glucocorticoid resistance in pediatric T-cell acute lymphoblastic leukemia through modulation of cholesterol biosynthesis and the WNT/β-catenin pathway

SUPPLEMENTARY DATA

Table S1: Sequences of primers used for RQ-PCR

PRIMER SEQUENCES	Forward	Reverse
Human *NFATc1*	TGCAAGCCGAATTCTCTGG	GGGAAGGTAGGTGAAACGCTG
Human *NFATc2*	GATAGTGGGCAACACCAAAGTCC	TCTCGCCTTTCCCGCAGCTCAAT
Human *NFATc3*	ACCAGGTGAAGGAACAGGTG	GCAATCTCCTTGCCACTCTC
Human *NFATc4*	ACAGTGAACCGACTGCAGAG	TGCAGATCACAGGCAGAAAC
Human *ABCB1*	GAATGTTCAGTGGCTCCGAG	TGTATGTTGGCCTCCTTTGC
Human *TSC22D3*	GGAATAGGTGCCAAGGATCTGG	GCTTACATCTGGTCTCATGCTGG
Human *BCL2L11*	GGTCCTCCAGTGGGTATTTCTCTT	ACTGAGATAGTGGTTGAAGGCCTGG
Murine *Nfatc1*	CCCGTCACATTCTGGTCCAT	GCTGTAGCGTGAGAGGTTCA
Murine *Nfatc2*	GGCATCCATGAGAACAGCAG	CGATGGTGGCTCTCATGTTG
Human *GUSB*	GAAAATATGTGGTTGGAGAGTTCATT	CGGAGTGAAGATCCCCTTTTTA
Murine *Gapdh*	GCAAAGTGGAGATTGTTGCCAT	CCTTGACTGTGCCGTTGAATTT

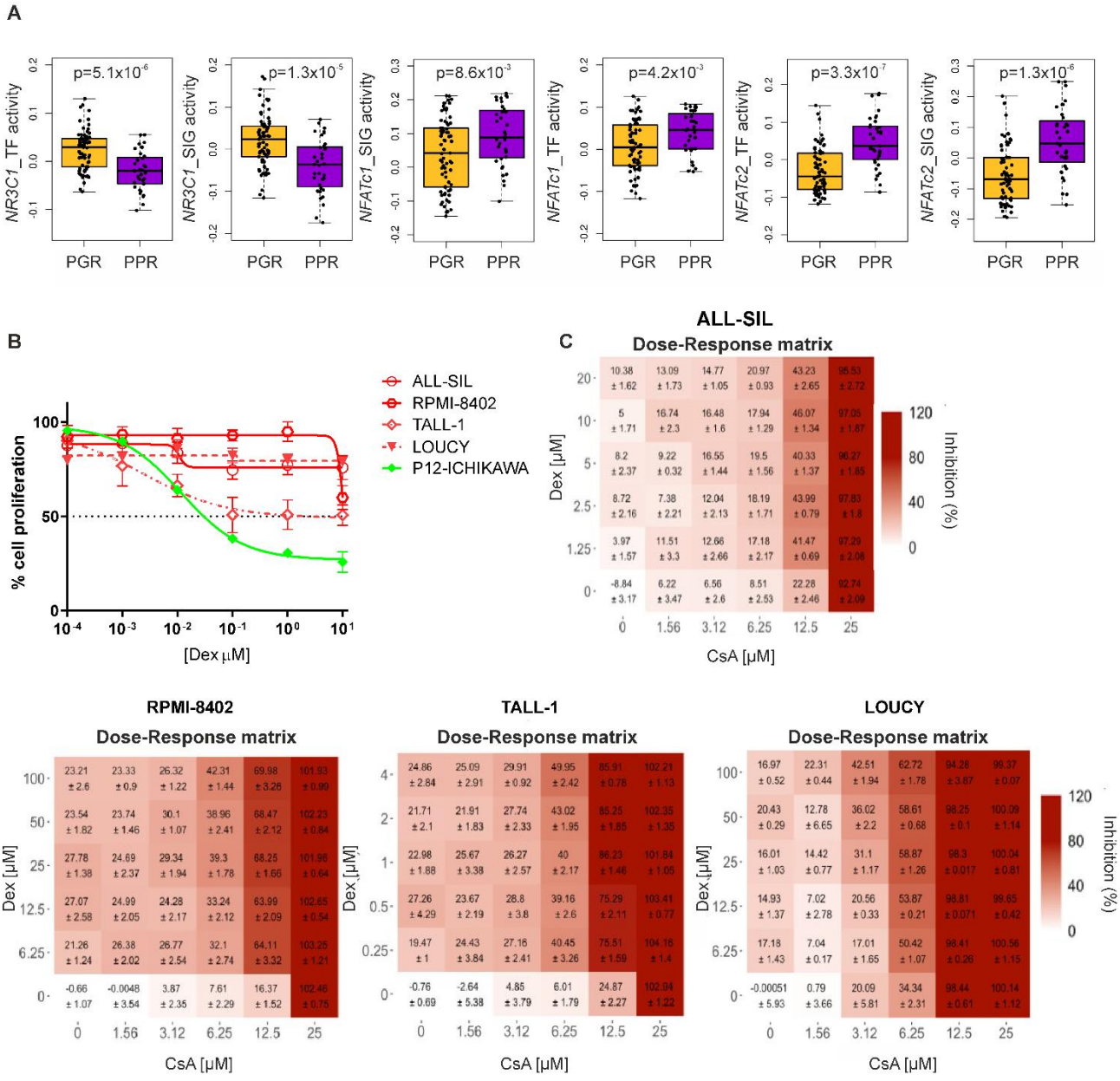
A
NR3C1_TF activity
p=5.1x10-6
NR3C1_SIG activity
p=1.3x10-5
NFATc1_SIG activity
p=8.6x10-3
NFATc1_TF activity
p=4.2x10-3
NFATc2_TF activity
p=3.3x10-7
NFATc2_SIG activity
p=1.3x10-6
PGR
PPR
B
% cell proliferation
[Dex µM]
ALL-SIL
RPMI-8402
TALL-1
LOUCY
P12-ICHIKAWA
C
ALL-SIL
Dose-Response matrix
Dex [µM]
CsA [µM]
Inhibition (%)
RPMI-8402
Dose-Response matrix
TALL-1
Dose-Response matrix
LOUCY
Dose-Response matrix
D
ALL-SIL
RPMI-8402
TALL-1
LOUCY
%AnnexV/PI-
DMSO
Cyclosporin A
Dex
Dex + Cyclosporin A

Figure S1: Diagnosed PPR T-ALL pediatric patients are characterized by high NFATc1 and NFATc2 transcriptional activity and signaling, whose inhibition by CsA reverts GC sensitivity. (A) Box plot showing the *NR3C1*, *NFATc1* and *NFATc2* transcriptional activity and signaling in PPR T-ALL pediatric patients compared to PGR one by NetBid2 inference (*NR3C1* TF activity p-value= $5.1*10^{-6}$; *NR3C1* SIG activity p-value=$1.3*10^{-5}$; *NFATc1* SIG activity p-value=$8.6*10^{-3}$; *NFATc1* TF activity p-value=$4.2*10^{-3}$; *NFATc2* TF activity p-value=$3.3*10^{-7}$; *NFATc2* SIG activity p-value=$1.3*10^{-6}$). (B) Percentage of cell proliferation measured by MTT assay in ALL-SIL, TALL-1, RPMI-8402 and LOUCY GC resistant cell lines treated with increasing concentrations of dex for 48 hours, $n \geq 3$ for all the experiments. (C) Dose-response matrix of cells' proliferation inhibition in ALL-SIL, RPMI-8402, TALL-1 and LOUCY GC resistant cells after 72 hours of treatment with CsA and dex. (D) Percentage of live cells (Annexin V/Propidium Iodide (PI) negative fraction) in ALL-SIL, RPMI-8402, TALL-1 and LOUCY cell lines treated with Growth Inhibition 50 (GI_{50}) value of CsA and dex for 72 hours. Results are presented as means + SEM (paired t test; ** $p < 0.01$; *** $p < 0.001$, **** $p < 0.0001$), $n \geq 3$ for all the experiments.

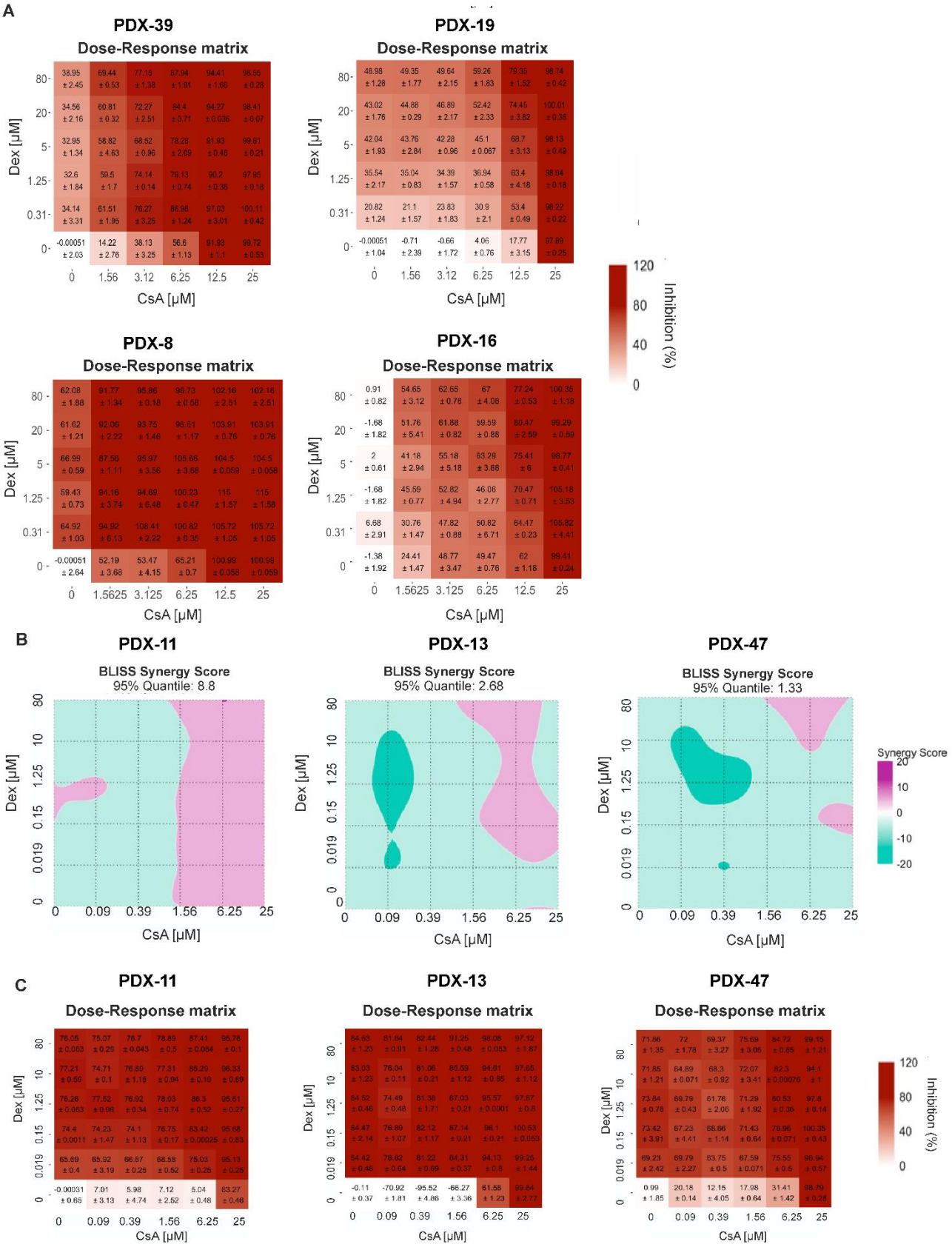
A
PDX-39
Dose-Response matrix
PDX-19
Dose-Response matrix
PDX-8
Dose-Response matrix
PDX-16
Dose-Response matrix
Dex [µM]
CsA [µM]
Inhibition (%)
B
PDX-11
PDX-13
PDX-47
BLISS Synergy Score
95% Quantile: 8.8
95% Quantile: 2.68
95% Quantile: 1.33
Synergy Score
C
PDX-11
PDX-13
PDX-47
Dose-Response matrix

Figure S2: In T-ALL GC sensitive cells, both CsA and dex synergize at high concentrations (A) Dose-response matrix of cells' proliferation inhibition in *ex vivo* primary cells from 4 GC resistant PDX mice after 72 hours of treatment with CsA and dex (B) 2D matrix representing Bliss synergy score of CsA and dex in reducing PDX GC sensitive cells' proliferation after 72 hours of treatment. (C) Dose-response matrix of cells' proliferation inhibition in *ex vivo* primary cells from 3 GC sensitive PDX mice after 72 hours of treatment with CsA and dex.

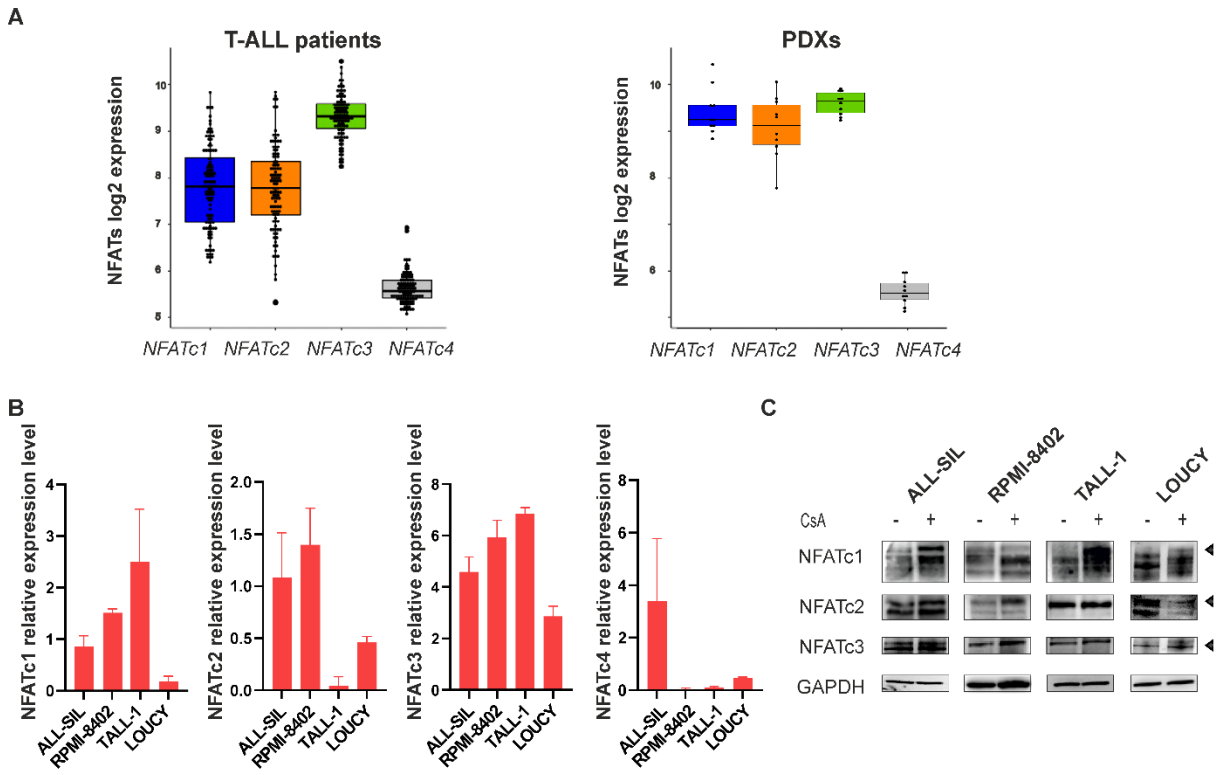

Figure S3: NFATs family expression levels. (A) *NFATc1*, *NFATc2*, *NFATc3* and *NFATc4 log2* expression levels obtained by transcriptome analysis in a cohort of 104 pediatric T-ALL patients at the diagnosis (on the left) and in 10 PDX T-ALL primary cells (on the right). (B) *NFATc1*, *NFATc2*, *NFATc3* and *NFATc4* expression normalized on *Glucuronidase Beta (GUS)* mRNA level in the four GC resistant T-ALL cell lines, measured by RQ-PCR; $n \geq 3$ for all the experiments. (C) Western Blot (WB) analysis of NFATc1, c2, c3 protein expression in ALL-SIL, RPMI-8402, TALL-1 and LOUCY cell lines treated with CsA GI_{50} for 1 hour.

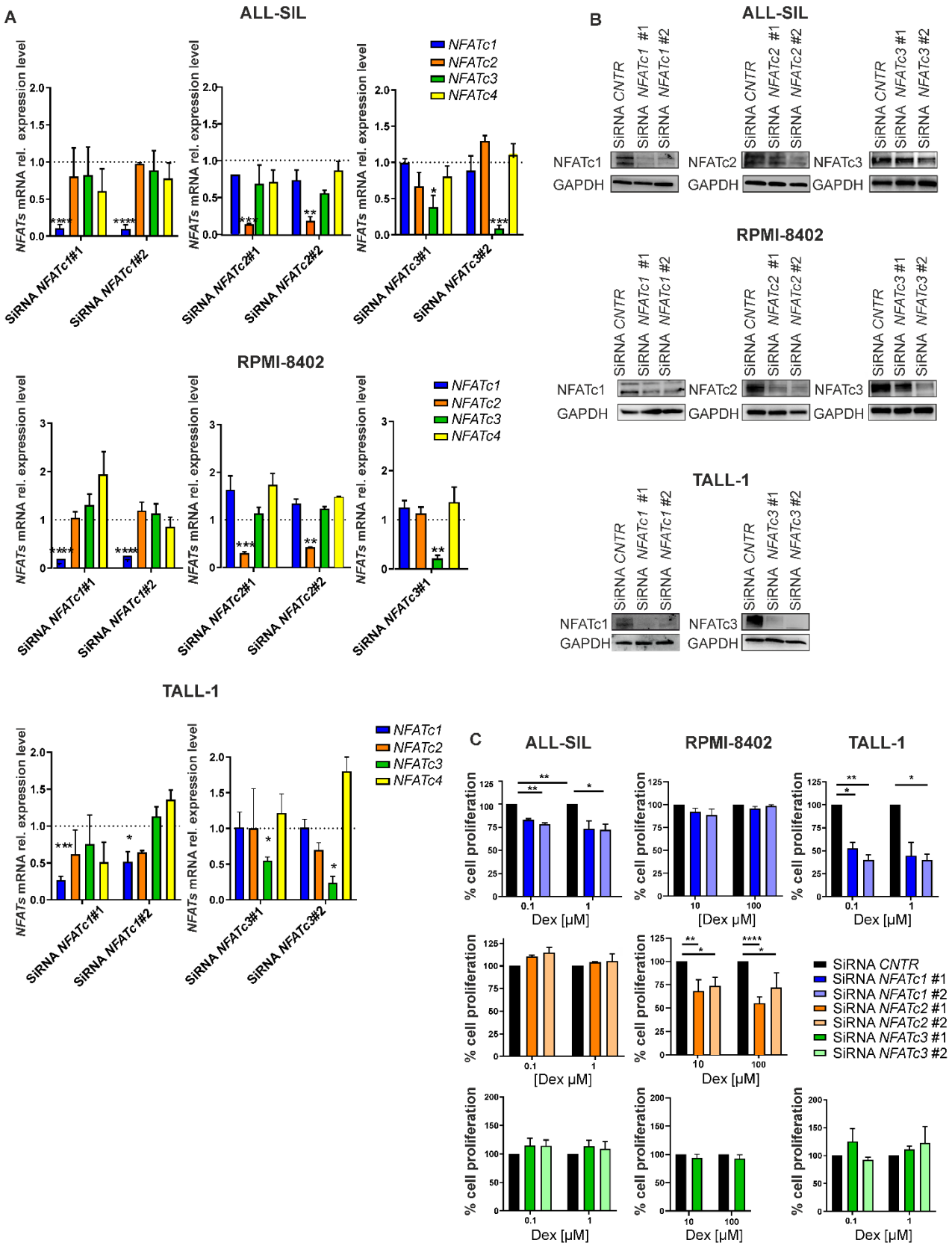
A
ALL-SIL
NFATs mRNA rel. expression level
NFATc1
NFATc2
NFATc3
NFATc4
SiRNA NFATc1#1
SiRNA NFATc1#2
SiRNA NFATc2#1
SiRNA NFATc2#2
SiRNA NFATc3#1
SiRNA NFATc3#2
RPMI-8402
TALL-1
B
ALL-SIL
SiRNA CNTR
SiRNA NFATc1 #1
SiRNA NFATc1 #2
SiRNA NFATc2 #1
SiRNA NFATc2 #2
SiRNA NFATc3 #1
SiRNA NFATc3 #2
NFATc1
NFATc2
NFATc3
GAPDH
RPMI-8402
TALL-1
C
ALL-SIL
RPMI-8402
TALL-1
% cell proliferation
Dex [μM]
SiRNA CNTR
SiRNA NFATc1 #1
SiRNA NFATc1 #2
SiRNA NFATc2 #1
SiRNA NFATc2 #2
SiRNA NFATc3 #1
SiRNA NFATc3 #2

Figure S4: Exclusively *NFATc1* or *NFATc2* specific gene silencing sensitizes T-ALL GC resistant cells to GC treatment. (A) *NFATs* mRNA expression levels measured by RQ-PCR after 24 hours of *NFATc1, c2 or c3* transient specific gene silencing with two different siRNAs in ALL-SIL, RPMI-8402 and TALL-1 cell lines. (B) WB analysis of NFATc1, c2, c3 and GAPDH protein after 48 hours from *NFATc1*, *c2* or *c3* transient gene silencing in ALL-SIL, RPMI-8402 and TALL-1 cells. (C) Percentage of cell proliferation in ALL-SIL, RPMI-8402 and TALL-1 cell lines transiently silenced for *NFATc1* (blue), *NFATc2* (orange) and *NFATc3* (green) gene expression after 48 hours of treatment with increasing concentration of dex. Results are presented as means + SEM (paired t-test; * $p < 0.05$; ** $p < 0.01$; *** $p < 0.001$; **** $p < 0.0001$), $n \geq 3$ for all the experiments.

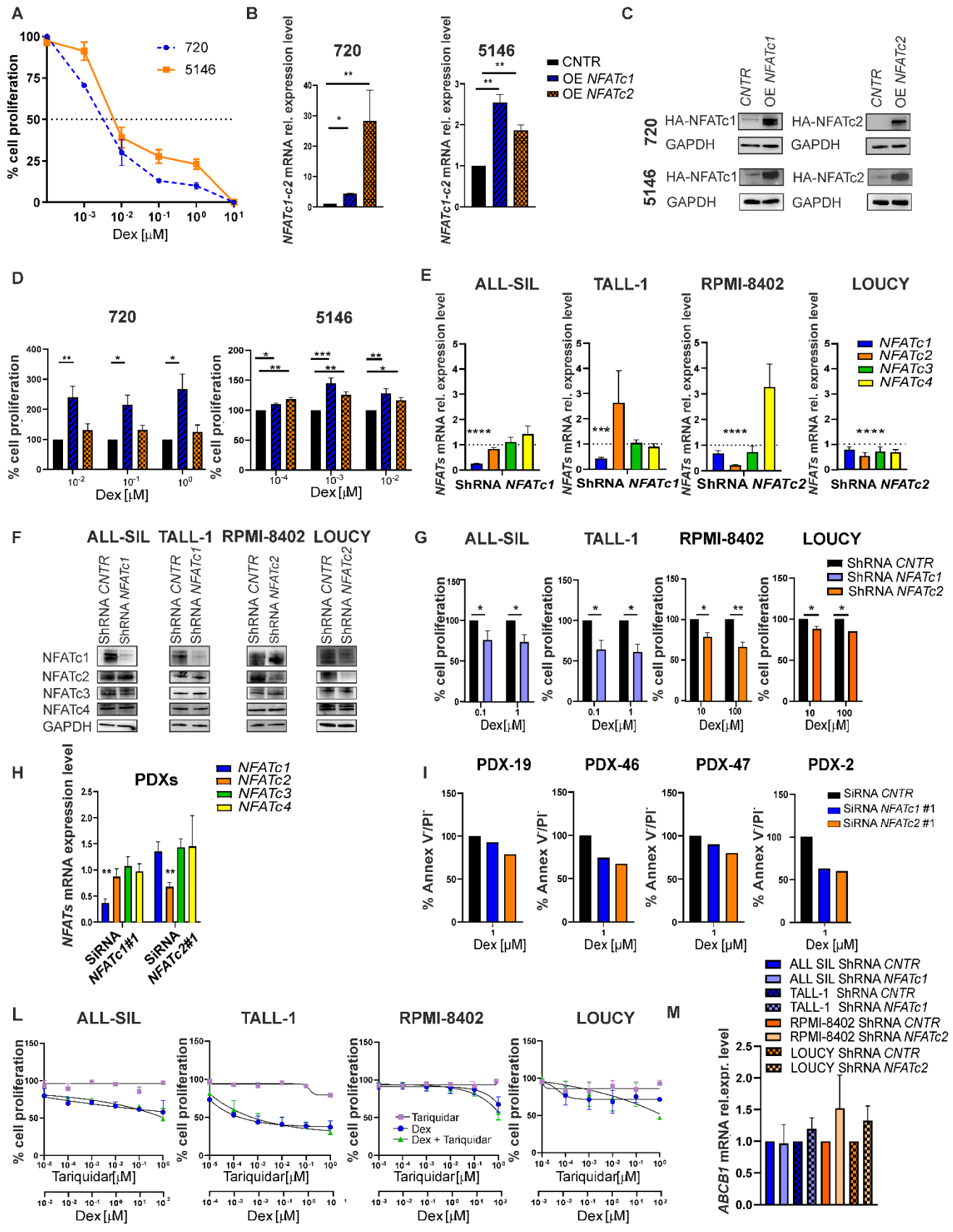
A
% cell proliferation
720
5146
Dex [μM]
B
720
5146
NFATc1-c2 mRNA rel. expression level
CNTR
OE NFATc1
OE NFATc2
C
CNTR
OE NFATc1
OE NFATc2
720
5146
HA-NFATc1
HA-NFATc2
GAPDH
D
720
5146
% cell proliferation
Dex [μM]
E
ALL-SIL
TALL-1
RPMI-8402
LOUCY
NFATs mRNA rel. expression level
ShRNA NFATc1
ShRNA NFATc2
NFATc1
NFATc2
NFATc3
NFATc4
F
ALL-SIL TALL-1 RPMI-8402 LOUCY
ShRNA CNTR
ShRNA NFATc1
ShRNA NFATc2
NFATc1
NFATc2
NFATc3
NFATc4
GAPDH
G
ALL-SIL
TALL-1
RPMI-8402
LOUCY
% cell proliferation
Dex[μM]
ShRNA CNTR
ShRNA NFATc1
ShRNA NFATc2
H
PDXs
NFATs mRNA expression level
NFATc1
NFATc2
NFATc3
NFATc4
SiRNA NFATc1#1
SiRNA NFATc2#1
I
PDX-19
PDX-46
PDX-47
PDX-2
% Annex V+/PI-
Dex [μM]
SiRNA CNTR
SiRNA NFATc1 #1
SiRNA NFATc2 #1
L
ALL-SIL
TALL-1
RPMI-8402
LOUCY
% cell proliferation
Tariquidar[μM]
Dex [μM]
Tariquidar
Dex
Dex + Tariquidar
M
ABCB1 mRNA rel.expr. level
ALL SIL ShRNA CNTR
ALL SIL ShRNA NFATc1
TALL-1 ShRNA CNTR
TALL-1 ShRNA NFATc1
RPMI-8402 ShRNA CNTR
RPMI-8402 ShRNA NFATc2
LOUCY ShRNA CNTR
LOUCY ShRNA NFATc2

Figure S5: NFATc1 and NFATc2 regulate T-ALL cells' response to GC without exploiting the ABC transporters. (A) Percentage of cell proliferation in 720 and 5146 cells treated with increasing concentration of dex for 48 hours. (B) *NFATc1-c2* mRNA expression level in 720 and 5146 CNTR and *NFATc1* or *c2* OE cells measured by RQ-PCR. (C) WB analysis of HA-*NFATc1* and HA-*NFATc2* and GAPDH proteins in 720 and 5146 CNTR and *NFATc1* or *c2* OE cells. (D) Percentage of cell proliferation in 720 and 5146 cells overexpressing (OE) *NFATc1* or *NFATc2* treated with increasing concentrations of dex for 48 hours. (E) *NFATs* mRNA expression level and (F) WB analysis of NFATc1, c2, c3 and GAPDH protein in stable ALL-SIL and TALL-1 ShRNA *NFATc1* knock-down cells as well as in RPMI-8402 and LOUCY *NFATc2* gene silenced cells and relative controls. (G) Percentage of cell proliferation in ALL-SIL and TALL-1 *NFATc1* knock-down (in blue) and in RPMI-8402 and LOUCY *NFATc2* knock-down (in orange) cells and relative controls treated with increasing concentration of dex. (H) *NFATs* mRNA expression level measured by RQ-PCR in PDXs after 24 hours from transient *NFATc1* or *NFATc2* gene silencing. (I) Percentage of viable cells in primary cells from 4 different PDXs after transient *NFATc1* and *c2* gene silencing and 48 hours 1 μM dex treatment. Results are presented as means + SEM (paired t-test; * $p < 0.05$; ** $p < 0.01$), $n \geq 3$ for all the experiments. (L) Percentage of cell proliferation in ALL-SIL, TALL-1, RPMI-8402 and LOUCY after 72 hours of treatment with scalar concentration of tariquidar alone or in combination with dex, $n \geq 3$ for all the experiments. (M) *ABCB1* mRNA relative expression level in ALL-SIL and TALL-1 ShRNA *NFATc1* cells and in RPMI-8402 and LOUCY ShRNA *NFATc2* knock-down cells and the relative controls, $n \geq 3$ for all the experiments.

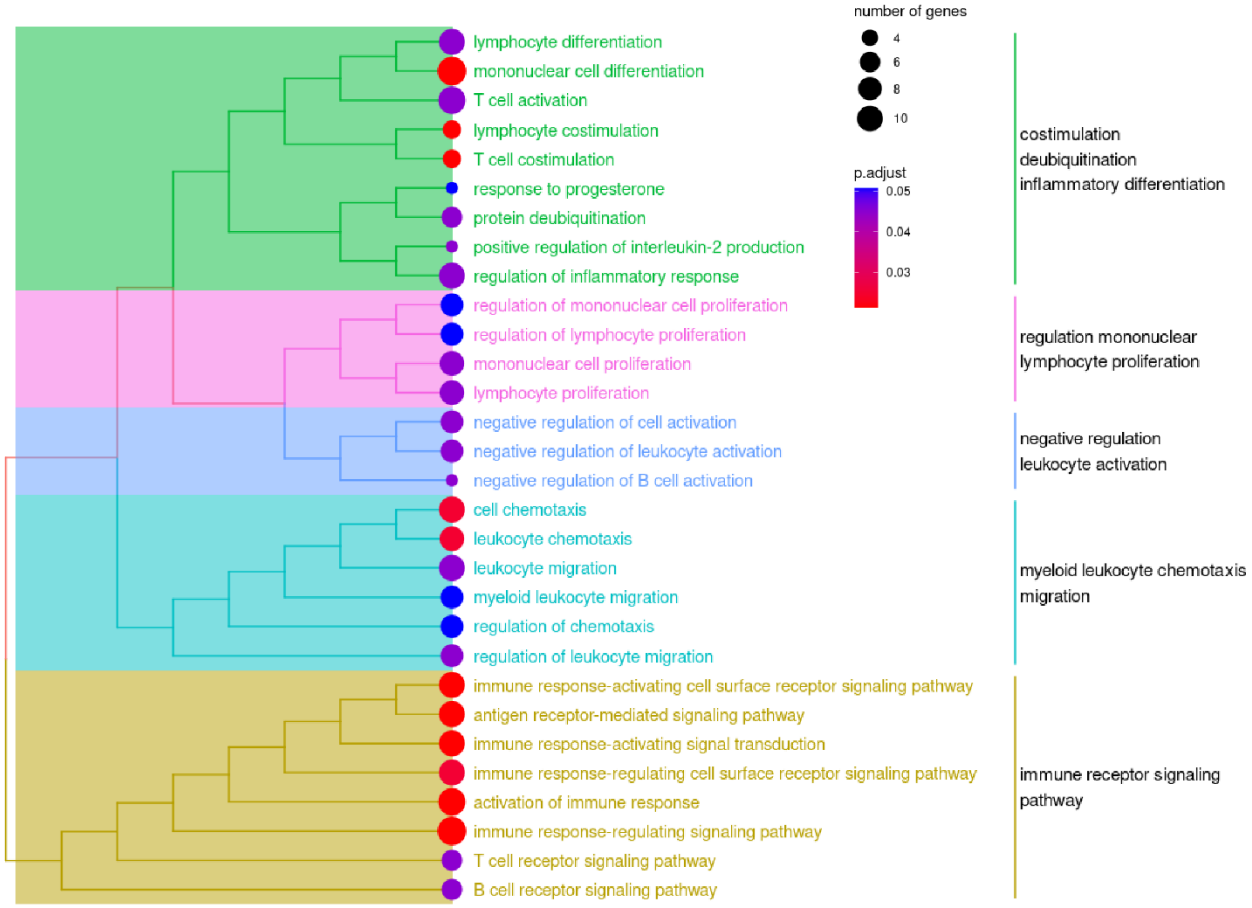

Figure S6: ***NFATc1* specific gene silencing upregulates genes involved in the negative T-cell activation.** Treeplots of over-represented GO-BP on upregulated in TALL-1 ShRNA *NFATc1* knock-down cells compared to controls. Dots size represents the gene count; circles color the adjusted p-value.

A

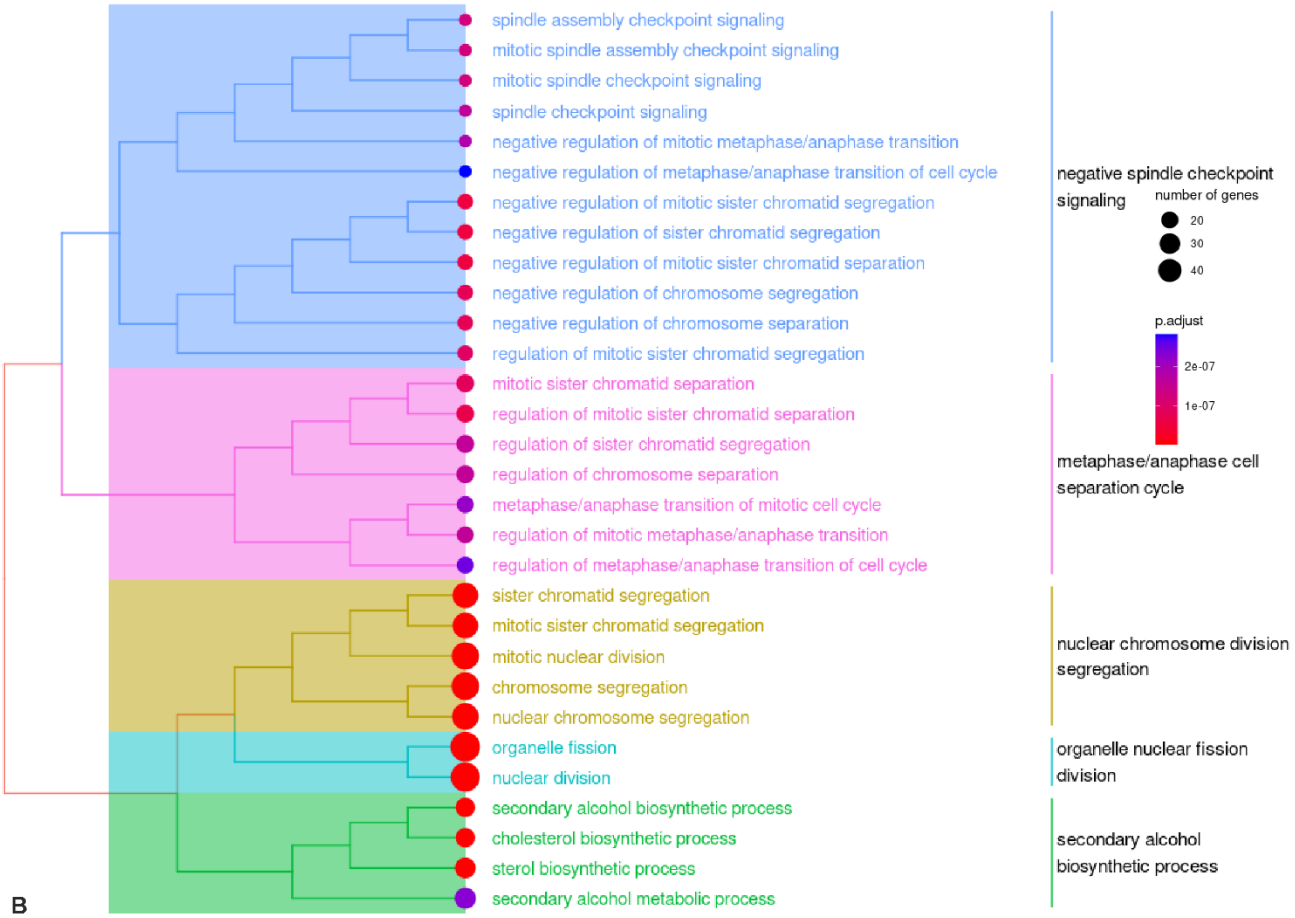
spindle assembly checkpoint signaling
mitotic spindle assembly checkpoint signaling
mitotic spindle checkpoint signaling
spindle checkpoint signaling
negative regulation of mitotic metaphase/anaphase transition
negative regulation of metaphase/anaphase transition of cell cycle
negative regulation of mitotic sister chromatid segregation
negative regulation of sister chromatid segregation
negative regulation of mitotic sister chromatid separation
negative regulation of chromosome segregation
negative regulation of chromosome separation
regulation of mitotic sister chromatid segregation
mitotic sister chromatid separation
regulation of mitotic sister chromatid separation
regulation of sister chromatid segregation
regulation of chromosome separation
metaphase/anaphase transition of mitotic cell cycle
regulation of mitotic metaphase/anaphase transition
regulation of metaphase/anaphase transition of cell cycle
sister chromatid segregation
mitotic sister chromatid segregation
mitotic nuclear division
chromosome segregation
nuclear chromosome segregation
organelle fission
nuclear division
secondary alcohol biosynthetic process
cholesterol biosynthetic process
sterol biosynthetic process
secondary alcohol metabolic process
negative spindle checkpoint signaling
number of genes
20
30
40
p.adjust
2e-07
1e-07
metaphase/anaphase cell separation cycle
nuclear chromosome division segregation
organelle nuclear fission division
secondary alcohol biosynthetic process

B

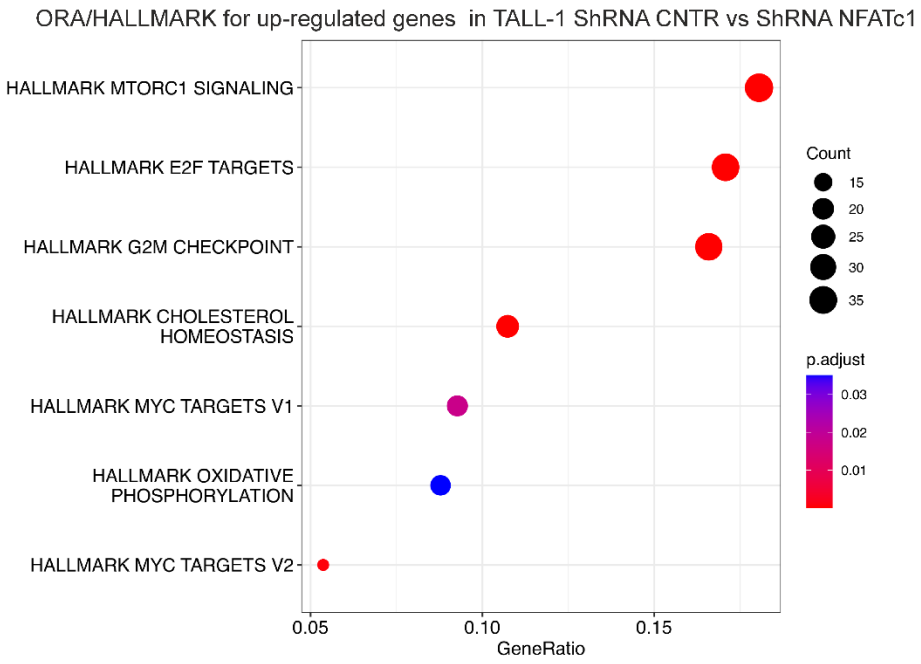
ORA/HALLMARK for up-regulated genes in TALL-1 ShRNA CNTR vs ShRNA NFATc1
HALLMARK MTORC1 SIGNALING
HALLMARK E2F TARGETS
HALLMARK G2M CHECKPOINT
HALLMARK CHOLESTEROL HOMEOSTASIS
HALLMARK MYC TARGETS V1
HALLMARK OXIDATIVE PHOSPHORYLATION
HALLMARK MYC TARGETS V2
0.05
0.10
0.15
GeneRatio
Count
15
20
25
30
35
p.adjust
0.03
0.02
0.01

Figure S7: ***NFATc1* specific gene silencing downregulates genes involved in cholesterol biosynthesis and MYC target.** (A) Treeplots of over-represented GO-BP on downregulated genes and (B) dot plot of downregulated hallmark MgSigDB gene sets in TALL-1 ShRNA *NFATc1* knock-down cells compared to controls. Dots size represents the gene count; circles color the adjusted p-value.

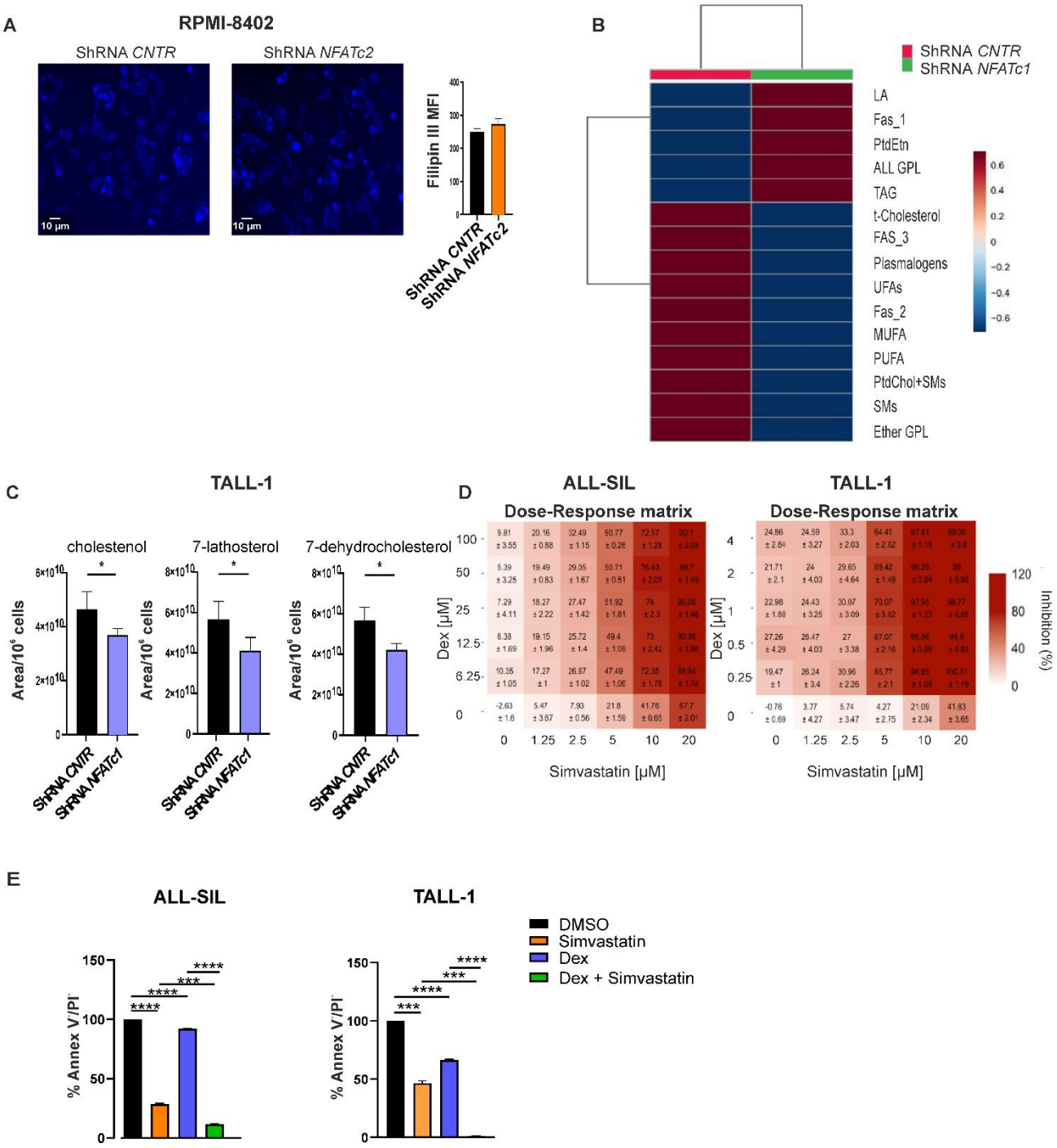

Figure S8: ***NFATc1* specific gene silencing downregulates intracellular cholesterol and simvastatin sensitizes T-ALL cells to dex treatment** (A) Intracellular unesterified cholesterol staining by Filipin III probe in RPMI-8402 ShRNA *NFATc2* knock-down cells and controls. On the right side Filipin III median MFI absolute quantification. (B) Heatmap of intracellular lipidome identified in organic fraction of TALL-1 ShRNA *CNTR* and TALL-1 ShRNA *NFATc1*. Abbreviations: Abbreviations: Fas, fatty acids: (Fas_1, Total Fatty Acyl chains at 1.56 ppm; Fas_2, methylene in FA at 1.29 ppm; Fas_3, ωCH3 methyl in FA at 0.89 ppm); GPL, glycerophospholipids; LA, Linoleic acid; MUFA, monounsaturated fatty acids; PtdCho, phosphatidylcholine; PtdEtn, phosphatidylethanolamine; PUFAs, polyunsaturated

fatty acids; SM, sphingomyelin; TAG, triacylglycerides; total cholesterol (t-cholesterol) UFAs, unsaturated fatty acids. (C) Bar plots showing the level of intracellular cholestenol, 7-lathosterol and 7-dehydrocholesterol in TALL-1 ShRNA NFATc1 compared to control cells detected by NMR technology (paired t test; * $p < 0.05$). (D) Dose-response matrix of proliferation reduction in ALL-SIL and TALL-1 GC resistant cells after 72 hours of treatment with simvastatin and dex. (E) Percentage of cell viability of ALL-SIL and TALL-1 cell lines (Annexin V/Propidium Iodide (PI) negative fraction) treated with 10 μM and 20 μM simvastatin and 25 μM or 1 μM dex respectively for 72 hours. Results are presented as means + SEM (paired t test; *** $p < 0.001$, **** $p < 0.000$), $n \geq 3$ for all the experiments.

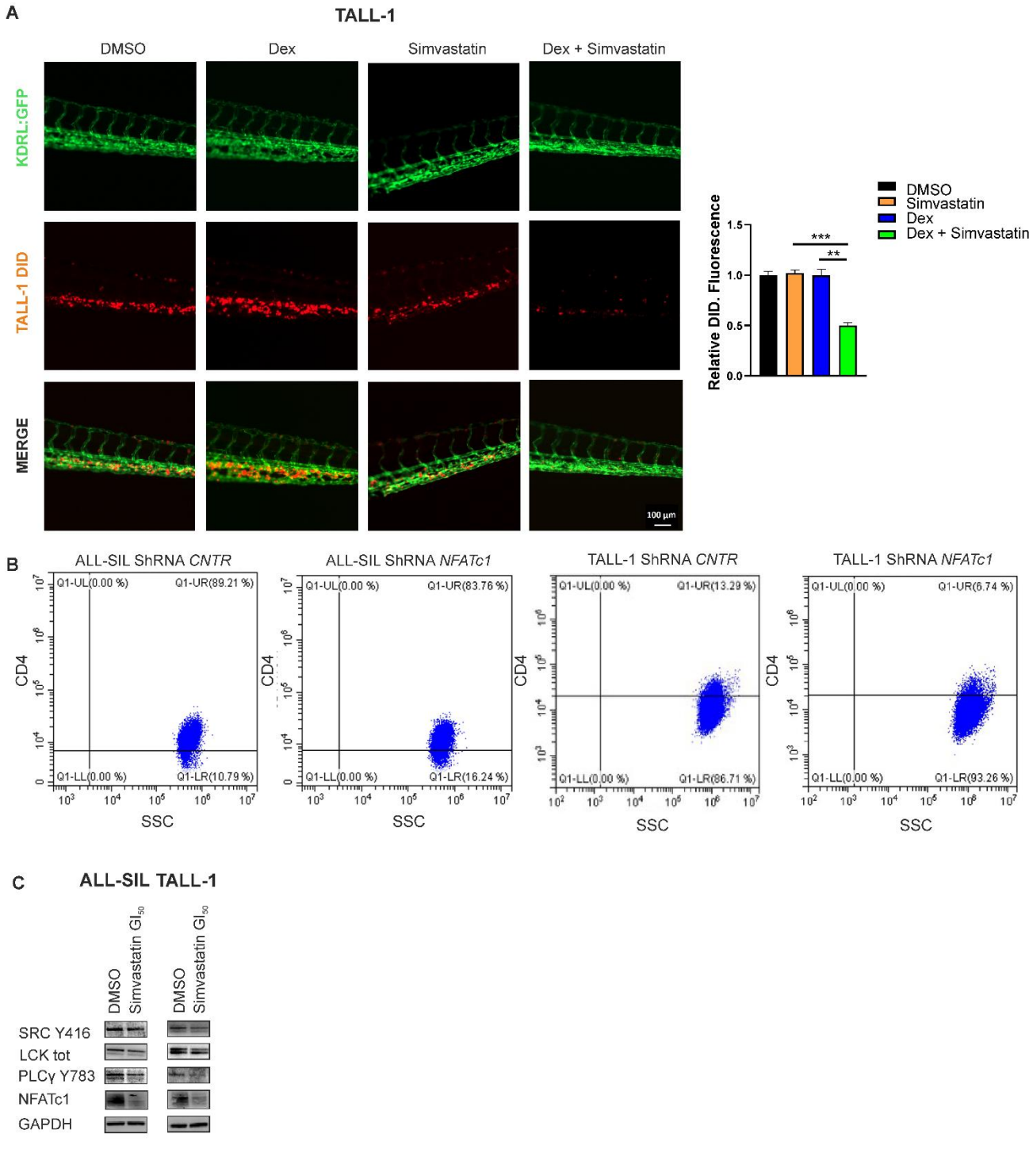
A
TALL-1
DMSO
Dex
Simvastatin
Dex + Simvastatin
KDRL:GFP
TALL-1 DID
MERGE
100 µm
Relative DID. Fluorescence
DMSO
Simvastatin
Dex
Dex + Simvastatin
***
**
B
ALL-SIL ShRNA CNTR
ALL-SIL ShRNA NFATc1
TALL-1 ShRNA CNTR
TALL-1 ShRNA NFATc1
CD4
SSC
Q1-UL(0.00 %)
Q1-UR(89.21 %)
Q1-LL(0.00 %)
Q1-LR(10.79 %)
Q1-UR(83.76 %)
Q1-LR(16.24 %)
Q1-UR(13.29 %)
Q1-LR(86.71 %)
Q1-UR(6.74 %)
Q1-LR(93.26 %)
C
ALL-SIL TALL-1
DMSO
Simvastatin GI50
SRC Y416
LCK tot
PLCγ Y783
NFATc1
GAPDH

Figure S9: **Simvastatin sensitizes T-ALL cells to dex treatment in the *in vivo* zebrafish model and negatively affects the TCR/LCK signaling** (A) Lateral view of the trunk region of Tg(Fli1:GFP) embryos injected with approximately 200 pre-labelled DiD^+ TALL-1 cells pre-treated *in vitro* with 20 μM Simvastatin or vehicle (DMSO) and then treated by adding dex directly into the fish water at a final 1 μM concentration or DMSO for 24 hours. On the right, quantification of the red intensity signal associated with transplanted cells. Scale bar, 100μm. Results are presented as means + SEM (unpaired t-test;** $p < 0.01$; *** $p < 0.001$), $n \geq 3$ for all the experiments. (B) Representative dot plots showing the number of $CD4^+$ cells in ALL-SIL and TALL-1 ShRNA *NFATc1* knock down cells and control cells. (C) WB analysis of NFATc1, SRC Y416, total LCK and PLCγ Y783 protein expression in ALL-SIL and TALL-1 treated with the respective GI_{50} value of simvastatin for 48 hours.

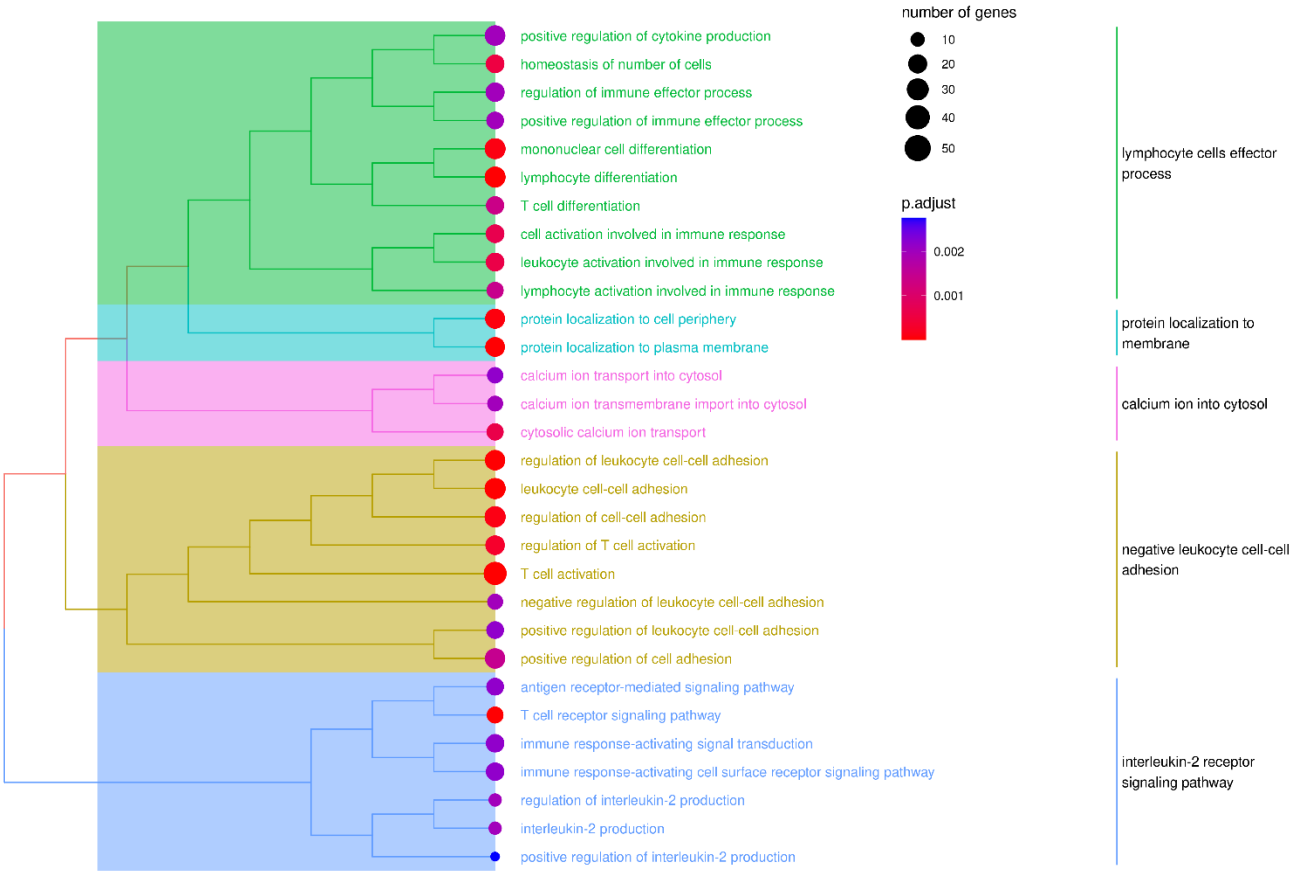

Figure S10: ***NFATc2* gene silencing induces T-cell differentiation.** (A) Treeplot showing upregulated GO-BP obtained by ORA in RPMI-8402 ShRNA *NFATc2* knock-down cells compared to controls. Filled circles size represents the number of genes; circles color the adjusted p-value.

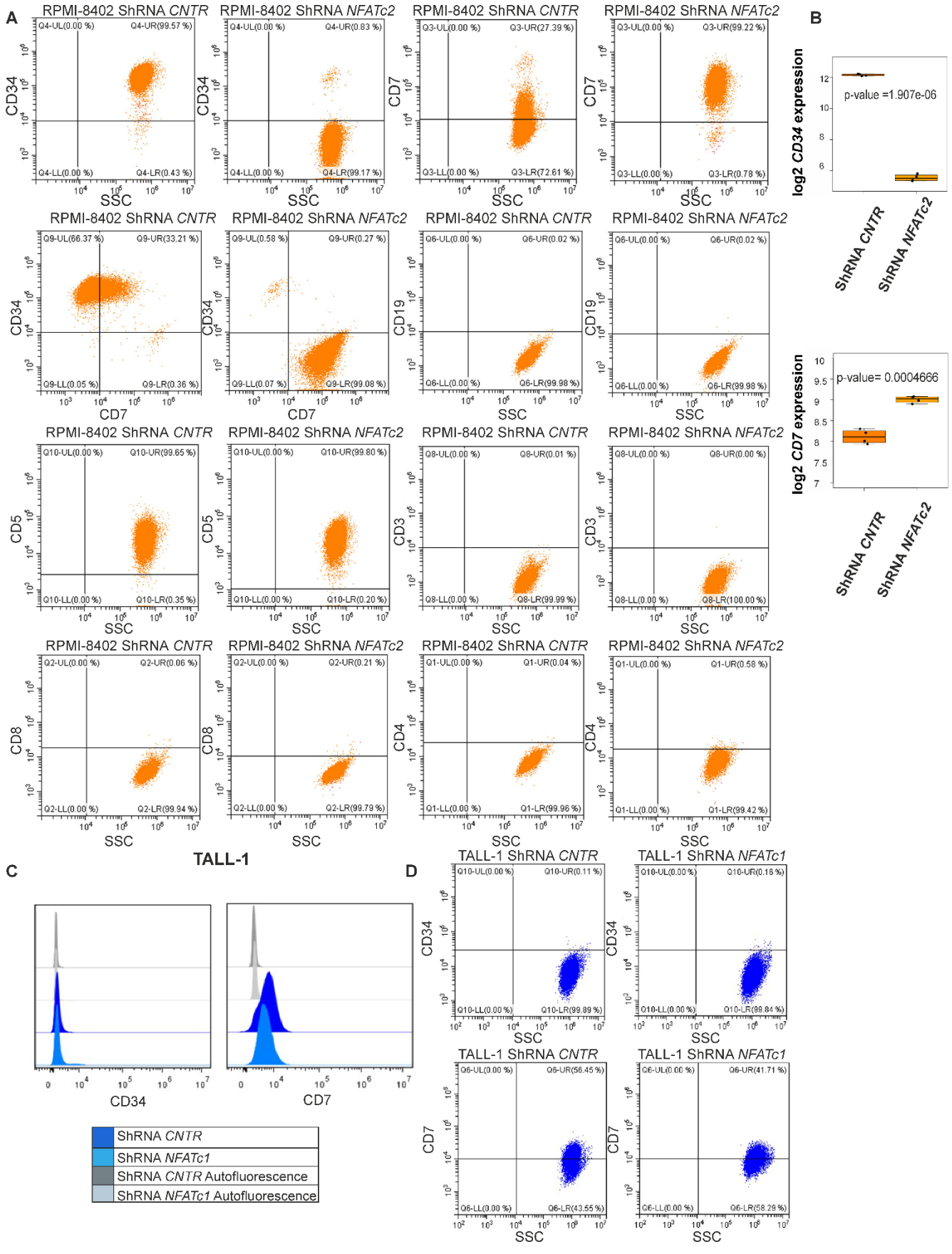
A
RPMI-8402 ShRNA CNTR
RPMI-8402 ShRNA NFATc2
CD34
CD7
CD19
CD5
CD3
CD8
CD4
SSC
B
log2 CD34 expression
p-value =1.907e-06
log2 CD7 expression
p-value= 0.0004666
ShRNA CNTR
ShRNA NFATc2
TALL-1
C
CD34
CD7
ShRNA CNTR
ShRNA NFATc1
ShRNA CNTR Autofluorescence
ShRNA NFATc1 Autofluorescence
D
TALL-1 ShRNA CNTR
TALL-1 ShRNA NFATc1

Figure S11: **Exclusively *NFATc2* gene silencing decreases the percentage of CD34$^+$ T-ALL cells and increases the CD7$^+$ one.** (A) Representative dot plots of CD34$^+$, CD7$^+$, CD5$^+$, CD3$^+$, CD8$^+$, CD4$^+$, CD19$^+$ RPMI-8402 ShRNA *NFATc2* knock down cells and controls and CD34$^+$ signal in relation to CD7$^+$ one. (B) *CD34* and *CD7* mRNA $\log_2$ value expression obtained from GEP analysis in RPMI-8402 ShRNA *NFATc2* knock down cells compared to controls (*CD34* p-value= 1.907 *10^6; *CD7* p-value= 0.0004666, Welch t-test). (C) Representative histogram showing the intensity expression of CD34$^+$ and CD7$^+$ cells in TALL-1 ShRNA *NFATc1* knock-down and control cells. (D) Representative dot plots of CD34$^+$ and CD7$^+$ expression in TALL-1 ShRNA *NFATc1* knock down cells and controls.

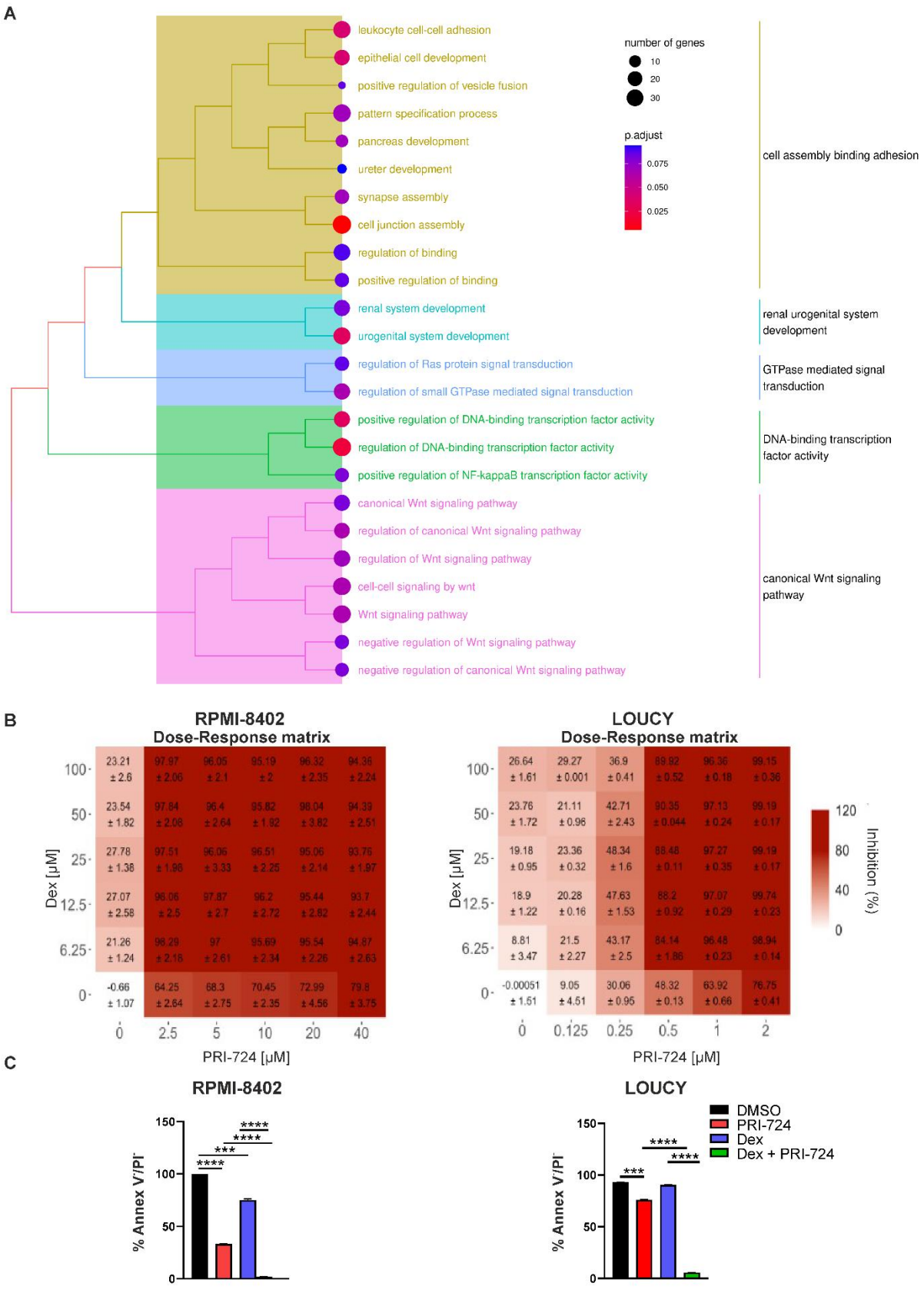
A
leukocyte cell-cell adhesion
epithelial cell development
positive regulation of vesicle fusion
pattern specification process
pancreas development
ureter development
synapse assembly
cell junction assembly
regulation of binding
positive regulation of binding
renal system development
urogenital system development
regulation of Ras protein signal transduction
regulation of small GTPase mediated signal transduction
positive regulation of DNA-binding transcription factor activity
regulation of DNA-binding transcription factor activity
positive regulation of NF-kappaB transcription factor activity
canonical Wnt signaling pathway
regulation of canonical Wnt signaling pathway
regulation of Wnt signaling pathway
cell-cell signaling by wnt
Wnt signaling pathway
negative regulation of Wnt signaling pathway
negative regulation of canonical Wnt signaling pathway
number of genes
10
20
30
p.adjust
0.075
0.050
0.025
cell assembly binding adhesion
renal urogenital system development
GTPase mediated signal transduction
DNA-binding transcription factor activity
canonical Wnt signaling pathway
B
RPMI-8402
Dose-Response matrix
LOUCY
Dose-Response matrix
Dex [μM]
PRI-724 [μM]
Inhibition (%)
C
RPMI-8402
LOUCY
% Annex V+/PI-
DMSO
PRI-724
Dex
Dex + PRI-724

Figure S12: *NFATc2* gene silencing negatively affects WNT/β-catenin pathway whose inhibition restores GC response in T-ALL cells. (A) Treeplot showing downregulated GO-BP obtained by ORA in RPMI-8402 ShRNA *NFATc2* knock-down cells compared to controls. Filled circles size represents the number of genes in over-represented terms, whereas circles color the adjusted p-value. (B) Dose-response matrix of proliferation reduction in RPMI-8402 and LOUCY GC resistant cells after 72 hours of treatment with PRI-724 and dex. (C) Percentage of cell viability in RPMI-8402 and LOUCY cells treated with PRI-724 and dex alone or in combination for 72 hours. Results are presented as means + SEM (paired t test; *** $p < 0.001$; **** $p < 0.0001$), $n \geq 3$ for all the experiments.

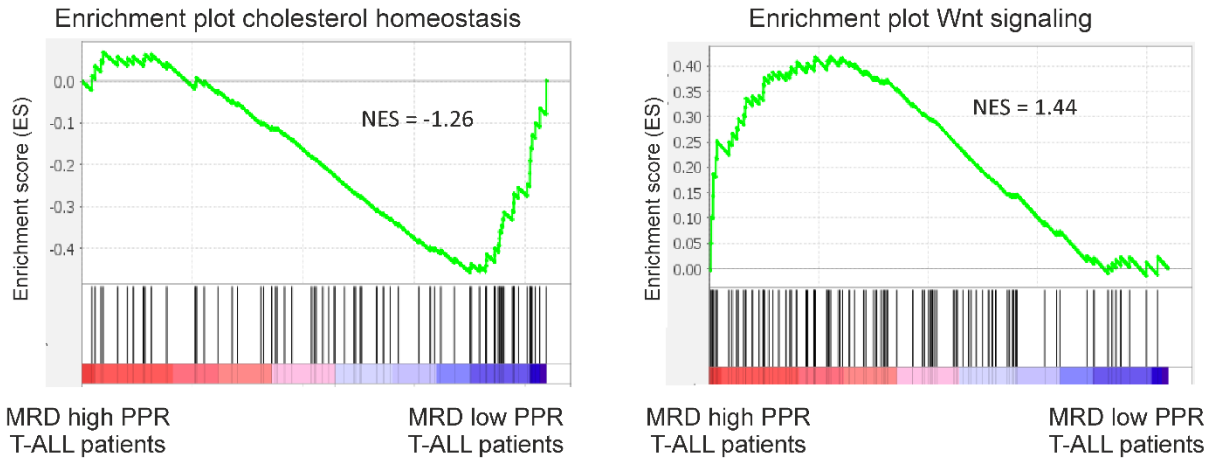

Figure S13: MRD positive and negative PPR T-ALL patients are characterized by an enrichment of genes belonging to Wnt signaling and cholesterol homeostasis respectively. GSEA for cholesterol homeostasis and Wnt signaling in MRD (+78) high and low PPR T-ALL pediatric patients at diagnosis (normalized enrichment score (NES) = -1.26 for cholesterol homeostasis, NES =1.44 for Wnt signaling, p.value<0.25.

EXTENDED METHODS

Cell culture

ALL-SIL (DSMZ, Braunschweig, Germany Cat# ACC-511), TALL-1 (DSMZ Cat# ACC-521), RPMI-8402 (DSMZ Cat# ACC-290, RRID:CVCL_1667), LOUCY (DSMZ Cat# ACC-394) P12-ICHIKAWA (DSMZ Cat# AC-34), 720 and 5146 cell lines were cultured in RPMI 1640 (Thermo Fisher Scientific, Waltham, MA, USA) with 10-20% Fetal Bovine Serum (FBS; Thermo Fisher Scientific), glutamine (2 mM/L; Thermo Fisher Scientific), penicillin (100 U/mL; Thermo Fisher Scientific) and streptomycin (100 mg/mL; Thermo Fisher Scientific) and maintained at 37°C in a humidified atmosphere with 5% CO_2. Each cell line was periodically tested for mycoplasma infection. All the human cell lines were purchased from DSMZ whereas the 720 and 5146 mouse cell lines were kindly gifted by Prof. Ntziachristos and Prof. Kelliher. Primary cells from patients derived xenograft (PDX) were cultured in minimum essential medium α (Thermo Fisher Scientific) with 10% FBS, 10% human serum (Thermo Fisher Scientific), penicillin (100 U/mL), human IL-7 (10 ng/mL; Peprotech, Cranbury, NJ, USA), human stem cell factor (50 ng/mL; Peprotech, Rocky Hill, NJ), human FLT3-ligand (20 ng/mL; Peprotech), and insulin (20 nM; Sigma-Aldrich, St. Louis, MO).

In vitro treatments

To assess GC sensitivity, ALL-SIL, TALL-1, RPMI-8402, LOUCY and P12-ICHIKAWA cell lines were treated with increasing concentration of dex dissolved in DMSO (D1756, Sigma-Aldrich,). Of note, the percentage of cell proliferation above or below 50% at 1 µM of dex was used as cut-off to select T-ALL

GC resistant and sensitive cell lines respectively [1]. ALL-SIL, TALL-1, RPMI-8402 SiRNA NFATc1, NFATc2 or NFATc3 and controls were treated with dex for 48 hours (0.1-1 μM for ALL-SIL and TALL-1, 10-100 μM for RPMI-8402). Similarly, ALL-SIL and TALL-1 ShRNA NFATc1, as well as RPMI-8402 and LOUCY ShRNA NFATc2 stable knock-down cells were treated with increasing concentration of dex (0.1-100 μM) for 48 hours. The 720 and 5146 mouse T-ALL cell lines overexpressing NFATc1 or NFATc2 and controls were treated with increasing concentration of dex (0.0001-1 μM). ALL-SIL, TALL-1, RPMI-8402 and LOUCY cell lines were treated with increasing concentration of tariquidar and dex alone or in combination for 72 hours. To assess the influence of cholesterol in GCs response, ALL-SIL and TALL-1 NFATc1 knock-down cells as well as the control cells were cultivated or not in medium plus cholesterol 1X (S5442, Sigma-Aldrich) for 24 hours, followed by 48 hours of dex (1-10 nM) treatment in normal medium or in medium plus cholesterol 1X. Similarly, RPMI-8402 and LOUCY cell lines were pre-treated with exogenous WNT3a ligand 30 ng/mL for 24 hours and followed by dex (0.1-10 μM) for 48 hours. Cell proliferation after all treatments was assessed by the MTT test.
To assess the impact of Calcineurin/NFAT pathway inhibition by CsA in combination with GC on T-ALL cells' viability , ALL-SIL, TALL-1, RPMI-8402 and LOUCY cell lines were treated with the CsA GI_{50} value (6,2 μM ALL-SIL, 2 μM TALL-1, 15 μM RPMI-8402 and 8 μM LOUCY) and a fixed concentration of dex (10 μM ALL-SIL, 1 μM TALL-1, 50 μM RPMI -8402 and 8 μM LOUCY) for 72 hours. Primary T-ALL cells derived from PDXs transiently silenced for NFATc1 or NFATc2 were treated with 1 μM dex, after 24 hours of siRNA transfection. Similarly, to evaluate the effect of cholesterol biosynthesis and WNT/β-catenin signaling inhibition in combination with dexamethasone on T-ALL GC resistant cells' viability, ALL-SIL and TALL-1 were treated with 10 μM simvastatin for 24 hours and then treated with dex (25 μM ALL-SIL and 1 μM TALL-1), RPMI-8402 and LOUCY cell lines were pre-treated with 2.5 μM and 1 μM PRI-724 respectively for 24 hours and then treated with 6.25 μM dex for 48 hours. Apoptosis of cell lines treated with CsA, simvastatin, PRI-724 alone or in combination with dexamethasone, as well as in NFATc1 or NFATc2 silenced cells was assessed by the AnnexinV–FLUOS staining kit.

Transcriptome analysis

Transcriptome data from 104 T-ALL pediatric patients at diagnosis, belonging to the AIEOP-BFM ALL2000/R2006 therapeutic protocol, and 10 T-ALL patient derived xenograft (PDX) were available and previously collected [2,3]. GEP data were obtained by GeneChip Human Genome U133 Plus 2.0 assays, normalized using RMA algorithm and processed with sva R package for batch effect removal. NetBID2 (v2.0.3, https://jyyulab.github.io/NetBID/) [4], a data-driven network-based inference pipeline was applied to identify driver transcription factors (TFs) and signaling factors (SIGs) in T-ALL patients. SJARACNe algorithm was applied with default parameters (IQR threshold 0.5 and IQR.loose_thre 0.1) to reconstruct the interactome, based on transcriptomic data. Then, NetBID2 allowed us to calculate TFs and SIGs expressions and activities, and to identify driver TFs and SIGs in PPR and PGR patients. In detail, Bayesian method was used for differential gene expression and driver activity analyses, with gaussian error distribution and pooling set to "full". Volcano plot was built using a customized function based on draw.volcanoPlot, setting logFC threshold to 0.03 and p-value threshold to 0.05. Pearson correlation was computed and represented using Hmisc (v5.1-0) and corrplot (v0.92) R packages. Hierarchical clustering analysis on patients was computed using Euclidean distance and Ward.d distance. Gene Set Enrichment Analysis (GSEA) between PPR HR vs non-HR patients according to MRD values at day +78, was

performed using “cholesterol homeostasis” and “WNT signaling” gene set in MSigDB database collection.

Total RNA was extracted from TALL-1 ShRNA *NFATc1* and from RPMI-8402 ShRNA *NFATc2* knock-down cells and controls after 12 hours of 1 μM and 10 μM dex treatment respectively using the RNeasy Mini Kit (Qiagen). Similarly, total RNA was extracted from P12-ICHIKAWA and TALL-1 cells treated or not with 1 μM dex for 12 hours. Next, the RNA was quantified using the Qubit RNA High Sensitivity Assay (Thermo Fisher Scientific) and the RNA quality was verified by Agilent 2100 Bioanalyzer (Agilent Technologies, Waldbronn, DE). Transcriptomic data were obtained using Clariom S Human arrays (Affymetrix, Santa Clara, CA, USA). Specifically, CEL files were normalized using the Robust Multichip Average (RMA) algorithm of the oligo-R package (v1.58.0). Differentially expressed genes (DEGs) in TALL-1 ShRNA *NFATc1* knock-down (470 genes downregulated and 114 upregulated) and RPMI-8402 ShRNA *NFATc2* knock-down cells DEGs (755 upregulated and 826 downregulated) were computed using Significant Analysis of Microarray R package (samr package, v3.0), with a False Discovery Rate (FDR) cut-off of 0.05. DEGs in P12-ICHIKAWA (142 upregulated and 95 downregulated) and TALL-1 cells (12 upregulated and 1 downregulated) treated or not with dex were computed using Linear Model for Microarray Data R package (limma R package, v3.50.3), adjusted p-value < 0.05. GSEA was performed in TALL-1 ShRNA *NFATc1* knock-down cells treated or not with dex, as well as in RPMI-8402 ShRNA *NFATc2* knock-down cells, in presence or absence of dex, using GSEA v4.2.2 with genes ranked by signal-to noise ratio and statistically significant gene sets determined by 1000 permutations and gene set permutations. Probe sets were collapsed to genes using max probe mode. A p-value cut-off of 0.05 was used in both the comparisons. MSigDB c5: GO:BP:Response to corticosteroid was used as tested gene set. Moreover, Over Representation Analyses (ORA) were applied to determine DEGs functional relationships of each comparison (i.e TALL-1 ShRNA *NFATc1* knock-down cells and the relative control, as well as for RPMI-8402 ShRNA *NFATc2* gene silenced cells compared to control ones). ORA analyses were performed with clusterProfiler R package (v4.2.2) using Gene Ontology (GO-BP) (www.geneontology.org) and MSigDB (www.gsea-msigdb.org) databases (c2: Chemical Genetic Perturbation (CGP) and Hallmarks) with an adjusted p-value cut-off of 0.1. The treeplot function (enrichplot v1.14.2 R package) was applied to generate ward.D hierarchical clustering after pairwise similarities of enriched terms calculated using JACCARD’S similarity coefficient (enrichplot v1.14.2 R package) and clusterProfiler. Data was deposited in the GEO repository at accession number: GSE254001.

Xenotransplantation model and *in vivo* drug treatment

The Tg(fli1: EGFP) zebrafish embryos were raised, staged, and maintained, as previously described [5,6]. Two-day-old Tg(fli1:EGFP) zebrafish embryos were anesthetized (0.003% tricaine) and positioned on 3% agarose. TALL-1 ShRNA *NFATc1*, RPMI-8402 ShRNA *NFATc2*, and control cells were labeled with Vybrant® DIL (Invitrogen) following the manufacturer’s protocol. Approximately 200 cells were resuspended in PBS (pH 7.4) and implanted using a pneumatic picopump equipped with borosilicate glass capillary needles (OD/ID: 1.00/0.75 mm, WPI, USA) within the duct of Cuvier of each embryo. After the injection procedure, the embryos were raised at 34°C and animals showing less than 100 cells after 2 hours from the transplant were discarded from the analysis. The TALL-1 ShRNA *NFATc1* and ShRNA *CNTR* injected embryos were incubated with 1 μM dex dissolved in fish water (0.3 g/L “Instant Ocean” Sea Salts and 0.08 g/L $CaSO_4*2H_2O$), whereas the RPMI-8402 ShRNA *NFATc2* cells embryos

and relative controls were incubated with 10 μM dex and each animal was photographed live with a Zeiss LSM800 confocal microscope after 24 hours treatment. Similarly, non-fluorescent TALL-1 cells were pre-treated in vitro with 20 μM simvastatin, and labeled with the Vybrant® DiD cell-labeling solution (Invitrogen, Carlsbad, CA, USA), according to the manufacturer's instructions. Approximately 200 TALL-1 cells pretreated or not with simvastatin were resuspended in PBS (pH 7.4) and implanted in zebrafish embryos as previously described. Following, a treatment with 1 μM dex dissolved in fish water was performed. At least 30 embryos per group were analyzed from three independent experiments. Embryos incubated with DMSO only were used as control.

3-(4,5-dimethylthiazol-2-yl)-2,5-diphenyltetrazolium bromide (MTT) assay

The effect of drug treatments or NFATs gene silencing on cell lines and primary T-ALL cells' proliferation was measured using MTT assay. Specifically, an equal number of cells were plated in triplicate in a 96-well plate and incubated with 10 μl MTT (Sigma-Aldrich) for 4 hours. The Growth Inhibition 50 (GI_{50}, compound concentration required to inhibit cell proliferation by 50%) was calculated by plotting the data as a logarithmic function of (x) when viability was 50%. Control cells viability was set to 100%.

High-Throughput drug synergism screening (HTS)

The HTS was performed as previously described [7]. Briefly, 13000-20000 c/well of primary T-ALL cells derived from PDXs were seeded in 384-well plates in 18 μl of RPMI growth medium with 20% FBS, 10 ng/mL human IL-7, 50 ng/mL human stem cell factor, 20 ng/mL human FLT3-ligand and 20 nM insulin and were immediately pre-treated with 2 μl of 10X CsA. After 24 hours, cells were then treated with 2 μl of 10X dex as single treatments or in combination in a 6x6 matrix design. 7000c/well of GC resistant T-ALL cell line models were seeded in 384-well plates in 24 μl of complete RPMI growth medium. T-ALL cells were immediately pre-treated with 3 μl of 10X DRUG (Simvastatin for ALL-SIL and TALL-1 and PRI-724 for RPMI-8402 and LOUCY. After 24 hours, cells were treated with 3 μl of 10X dex as single treatments or in combination in a 6x6 matrix design. Each drug was tested in a 6-point 2-fold dose-response curve, and each dose was tested in duplicate within each plate, in two independent experiments. A gas-permeable sealing membrane (Breathe-Easy, Merck, Readington Township, NJ) was used to avoid evaporation during treatment incubation. After 48 hours of treatment, 3 μl of resazurin (10X) was added to each well to reach a final concentration of 44 μM, incubated for 3 hours at 37°C, and then the fluorescence signal was measured at 590 nm using a multi-well plate reader (Spark, Tecan, Männedorf, Switzerland). To ensure treatment reproducibility, all procedures, including cell seeding, drug dilutions, cell treatments and application of resazurin solution, were carried out through a 96-channel robotic liquid handler (Microlab STAR 96-CORE, Hamilton, Bonaduz, Switzerland). The Z-prime (Z') quality control metrics were calculated for each plate to measure the separation between the positive control (1 μM bortezomib) and negative control (0.5% DMSO). For this screening, only plates with acceptable quality metrics (Z' > 0.4) were further analyzed. Raw data were normalized according to the following equation: cell viability (%) = $x-POSNEG-POS*100$, where x is the relative fluorescence units (RFU) collected from each single well, NEG is the mean of intraplate negative controls (0.5% DMSO) and POS is the mean of intraplate positive controls (1 μM bortezomib). SynergyFinder R package was applied to compute the Bliss synergy score.

Annexin V/Propidium Iodide (PI) staining

Annexin V–FLUOS staining kit (Roche, Basel, Switzerland) was used to detect the percentage of cell viability, apoptosis and necrosis of cell lines and primary cells treated with CsA, simvastatin or PRI-724 as well as in *NFATc1* or *NFATc2* silenced cells in combination with dexamethasone. Samples were

analyzed by flow cytometric analysis (Cytomics FC500, Beckman Coulter, CA). DMSO-treated cells' vitality was set to 100%.

NFATs transient and stable gene silencing and overexpression

For transient gene silencing, two different Small-interfering (si)RNA (Thermo Fisher Scientific, WLM, USA) sequences targeting the coding region of each NFAT member were used at 50 pM to selectively silence human *NFATc1, c2 or c3* gene. A negative control siRNA (stealth RNAiTM siRNA Negative Control, Thermo Fisher Scientific) was used as control in each experiment. Cell transfection was performed using the Nucleofector systems (Amaxa Biosystems, Lonza Sales Ltd., Basel, Switzerland) according to the manufacturer's instructions as previously described [8]. *NFATs* specific gene silencing was verified by RQ-PCR after 24 hours and by WB analysis after 48 hours from siRNA transfection. Specifically, *NFATc1*, *NFATc2* and *NFATc3* transient gene silencing was performed in ALL-SIL, TALL-1 and RPMI-8402, except for *NFATc2* gene silencing that was conducted only in ALL-SIL and RPMI-8402, since by RQ-PCR data *NFATc2* is not expressed in TALL-1. *NFATc1* or *NFATc2* stable gene knock-down was obtained employing lentiviral plasmids containing *NFATc1* or *NFATc2* short hairpin RNA (ShRNA) expression cassette and as reference a control ShRNA sequence (ShRNA *CNTR*) from a lentiviral construct carrying a scramble RNA (Merck, Darmstadt, DE). In detail, the viral particles were produced by transfecting 293T cells (ATCC, Manassas, VA) with the 2nd-generation packaging plasmids. Specifically, lentiviral vector-containing supernatants were collected after 48 hours of transfection, centrifuged to eliminate 293T cells and filtered with a 0.45 μM filter to discard any cellular debris. Viral particles were titrated by serial dilution on NIH-3T3 cells (DSMZ Cat# ACC-59, RRID: CVCL_0594). One microgram of p24 equivalent of lentiviral vector-containing supernatant was used to transduce $3*10^6$ cells, centrifuging at 32°C for 2.5 hours at 2500 Revolutions Per Minute (RPM). After infection, transduced cells were seeded and selected by culturing in medium with 1 μg/μL puromycin. *NFATc1* or *NFATc2* specific gene silencing was verified by RQ-PCR and by WB experiments. 720 and 5146 mouse T-ALL cells ($0.2*10^6$) were transduced, at the multiply of infection (MOI) 100, with the lentiviral vector PGK.GFP LV containing a GFP sequence and the *NFATc1* or *c2* mouse gene sequence conjugated with the human influenza hemagglutinin (HA) or with the control lentiviral vector containing the GFP tag sequence [9]. Transduction was performed in medium serum free for 12 hours. 720 and 5146 transduced cells have been left to grow at least for one week and then fluorescence-activated cell sorting (FACS) analysis was used to select GFP^+ cells and exclude the pseudo transduction products. *NFATc1* or *NFATc2* mRNA overexpression was verified by RQ-PCR and the increase in NFATc1 or c2 protein level was determined by WB using an anti-HA antibody.

Immunoblotting

Whole cell protein lysates were prepared in RIPA buffer (Sigma-Aldrich) plus protease and phosphatase inhibitors (Sigma-Aldrich) as previously described [10] and following the manufacturer's instructions. Protein concentration in each sample was assessed using the BCA protein assay (Thermo Fisher Scientific). Protein lysates were analyzed by SDS–polyacrylamide gel electrophoresis as previously described. The following primary antibodies were used: NFATc1 (Santa Cruz Biotechnology, CA, USA, Cat# sc-7294, RRID:AB_2152503) NFATc2 (Santa Cruz Biotechnology, Cat# sc-7296, RRID:AB_628012), NFATc3 (Abcam, CB, UK, Cat# ab245501), NFATc4 (Abcam, Cat# ab3447, RRID:AB_303809), SRC Y416 (Cell Signaling Technology, MA, USA, Cat # CS2101,), LCK (Cell Signaling Technology, Cat # CS2657 and CS2752), GAPDH (Genetex, Irvine, CA, USA, Cat# GTX 8627408), Phospholipase C Gamma (PLCγ Y783) (GeneTex Cat# GTX133465, RRID:AB_2886998), anti-HA (Abcam, Cat # ab1818,), β-catenin (Abcam, Cat # ab2365), LRP6 (Cell Signaling Technology,

Cat # CS2560), TCF-4 (Cell Signaling Technology, Cat # CS2569), HHEX (Abcam, Cat # ab79392), GR (Cell Signaling Technology, Cat# CSD4X9).

RNA extraction, cDNA synthesis and quantitative Real Time PCR

Total RNA was extracted with RNeasy Mini Kit (Qiagen, Hilden, DE) following the manufacturer's instruction. SuperScript II Reverse Transcriptase (Thermo Fisher Scientific) was used to retro transcribe 1 µg of RNA following the manufacturer's instruction. Gene expression was assessed by RQ-PCR using the QPCR Platinum Sybr Mix (Thermo Fisher Scientific). Relative gene expression was calculated using the $2^{-\Delta\Delta ct}$ method, normalizing to the expression of human *Glucuronidase Beta* (*GUSB*) or the murine *Glyceraldehyde 3-phosphate dehydrogenase* (*GAPDH*) and to the average ratio of control cells which was arbitrarily defined as 1. Primer sequences for each gene are reported in Table S1.

GR-luciferase assays

The GR luciferase reporter plasmids GR-GRE-luciferase reporter was kindly donated by Prof. De Bosscher (Ghent University). TALL-1 and ALL-SIL cells expressing control or ShRNA *NFATc1*, as well as RPMI-8402 and LOUCY cells expressing ShRNA *NAFTc2* or control, were transiently transfected via electroporation with the GR-GRE-luciferase reporter plasmid and the pMAXGFP control vector. Briefly, cells were washed with PBS, and 3.0×10^6 cells per transfection were resuspended in Ingenio® Electroporation Solution (Mirus, WI, USA) with a total of 5 µg plasmid DNA (4 µg GR-GRE-luciferase and 1 µg pMAXGFP). Electroporation was performed using the Amaxa Nucleofector system according to the manufacturer's protocol, as previously described[10]. Following electroporation, cells were seeded at 1×10^6 cells/mL in complete medium and, after 24 hours, treated with 10 µM dexamethasone or DMSO for 6 hours. Luciferase and GFP signals were measured using a Spark Tecan plate reader. The GFP signal was used to control for transfection efficiency and to normalize luciferase activity across samples. GR transcriptional activity was expressed as the ratio of normalized luciferase signal in dexamethasone-treated cells versus DMSO-treated controls.

Filipin III staining

Intracellular cholesterol amount in ALL-SIL and TALL-1 ShRNA *NFATc1* knock-down as well as in RPMI-8402 ShRNA *NFATc2* knock-down and in the relative control cells was assessed by Cholesterol Cell-Based Detection Assay Kit (Cayman Chemical, MI, USA) according to manufacturer's instructions. Briefly, $1.5*10^4$ ALL-SIL and TALL-1 ShRNA *CNTR* and ShRNA *NFATc1* as well as RPMI-8402 ShRNA *CNTR* and ShRNA *NFATc2* cells were seeded in a 96-well plate pre-coated for 30 minutes with 1 mg/mL of fibronectin to let the cells attach to the plate. Cells were cultivated overnight and fixed with the Cell-Based Assay fixative solution for 10 minutes. Subsequently, cells were incubated with Filipin III probe. Signal was assessed using an excitation of 340-380 nm and an emission to 385-470 nm. Filipin III Median Fluorescence Intensity (MFI) for each image of ALL-SIL and TALL-1 ShRNA *NFATc1* knock-down and controls as well as RPMI-8402 ShRNA *CNTR* and ShRNA *NFATc2* were calculated using the ImageJ software.

Nuclear Magnetic Resonance (NMR) spectroscopy

For the extraction of lipid metabolites, TALL-1 ShRNA *CNTR* and ShRNA *NFATc1* cell pellets were processed as previously described [11]. Briefly, the dried organic samples were resuspended in 750 µL of solution CDCl3:CD3OD (2:1; v/v), containing 0.02% tetramethylsilane (TMS) for chemical shift for NMR analyses. 1H-NMR analyses were performed at 25°C at 600 MHz (14.1 T Bruker AVANCE Neo spectrometer; Karlsruhe, Germany, Europe) on organic cell extracts using standard 1D Bruker library 1H NMR spectra. A total of 512 scans were collected into 32,768 data points using a spectral width of

12500 Hz, an acquisition time of 1.31 s and a relaxation delay (d1) of 5 seconds. Prior to Fourier transformation, each FID (free induction decay) was zero-filled to 65,536 points and multiplied by a 0.3 Hz exponential line-broadening function. Subsequently, spectra were manually phased, baseline corrected, and chemical shifts referenced internally to TMS at d = 0.00 ppm by using Topspin software 4.1. Relative quantification (area) of lipid signals in organic fractions was normalized to the number of cells. Heatmap and multivariate analyses were performed by MetaboAnalyst5.0 tool. An unpaired two-tailed Student t-test was applied for the comparison between NMR data groups.

ChIP and droplet digital PCR (ddPCR) analysis

ChIP experiments were performed as described previously [12]. Briefly, $25*10^6$ of TALL-1 or RPMI-8402 cells were crosslinked with 1% of formaldehyde for 10 minutes and lysed in lysis buffer plus protease inhibitors (50 mM Hepes-KOH, 7.5pH, 1 mM EDTA, 140 mM NaCl, 10% glycerol, 0.5% NP-40 and 0.25% Triton X-100) for 10 minutes at 4°C. Next, the nuclei were lysed in nucleus lysis buffer (10 mM TRIS HCl, 1 mM EDTA, 0.1% SDS), followed by sonication using Covaris M220 Focused-ultrasonicator instrument to obtain DNA fragments. A preclearing step of chromatin was performed, incubating the total amount of sonicated chromatin with 75 µl of protein G Dynabeads (Thermo Scientific) in reaction buffer. Contemporary, protein G Dynabeads were incubated with 2.5 ug of NFATc1 or 7.5 ug of NFATc2 and an equal amount of IgG as negative control for 8 hours and 4°C then washed with a buffer (0.01% SDS, 1.1% Triton X-100, 1.2 mM EDTA, 16.7 mM Tris-HCl 8.1pH, 167 mM NaCl). Next, beads-antibody complexes and sonicated chromatin were incubated overnight at 4°C with rotation. Complexes bound to the beads were washed using buffers with increasing salt concentration: 2X with Low Salt Buffer (0.1% SDS, 1% Triton X-100, 2 mM EDTA, 20 mM Tris-HCl 8.1pH, 150 mM NaCl), 1X with High Salt buffer (0.1% SDS, 1% Triton X-100, 2 mM EDTA, 20 mM Tris-HCl 8.1pH, 500 mM NaCl) and 1X with TE buffer (100 mM Tris-HCl 8.1pH, 1 mM EDTA). After the last washing step, the ChIP DNA was eluted by resuspending the chromatin-antibody-beads complexes in elution buffer (100 mM NaHCO3, 1% SDS) at 65°C for 15 minutes, followed by treatment with RNase and proteinase K. The crosslinks were then reversed, and the DNA was precipitated using ethanol and glycogen.

To investigate the molecular binding of NFATc1 and NFATc2 to specific DNA sequences we analyzed NFATc1 or NFATc2 ChIP samples by ddPCR technique using EvaGreen Digital PCR Supermix (Bio-Rad) and the following couples of primers self-designed based on JASPAR (https://jaspar.uio.no) predicted NFATc1 or c2 DNA binding sequence:

GENE

PRIMER SEQUENCE
NFATc1/c2 DNA BINDING SEQUENCE

Hmgcs1

F: TGTCTGCCCAGGTGATGAAAATTTCCA

R: CCTTTCACTTCAGCCTCCCT

Dhcr7

F: TGCTCAAACAGAAACCAAACCATGGAAA

R: GGACCTACCCTCTCAGTGTC

Ebp

F: TTTGATCAGGGCAGGGACAGTGGAAA

R: TCCCACTCAGAGCAACCAAT

Lrp6

F: TTGCAGTGTTTCCCCATTCGTTTTCCT

R: TCTTTGCTGACTCCTCCCAT

The promoter region of *MyoD* gene served as negative control [13]:

MyoD F: CTCTGCTCCTTTGCCACAAC; *MyoD* R: GAGTGCTCTTCGGGTTTCAG.

Specifically, each sample was emulsified to obtain droplets that were processed in a standard thermal cycler according to manufacturer's instructions. Next, the QX200 Droplet Digital PCR (ddPCR™) System (Bio-Rad) was used to analyze the amplification signals for each sample (NFATc1 or NFATc2 ChIP samples and IgGs). The quantity of DNA was measured as DNA copies/µl and normalized on the relative IgG sample, obtaining the enrichment over IgG ratio plotted on bar graphs.

Lipid Rafts (LRs) staining

To detect plasma membrane LRs in ALL-SIL and TALL-1 ShRNA *NFATc1* knock-down cells and controls, the Vybrant™ Alexa Fluor™ 488 Lipid Raft Labeling Kit (Thermo Fisher Scientific) was employed according to the manufacturer's instructions. Images were captured by the Zeiss LSM800 Airyscan microscope and the number of LRs for each cell was analyzed by ImageJ software.

LCK staining

ALL-SIL and TALL-1 ShRNA *NFATc1* knock-down and control cells were stained for LCK expression by immunofluorescence (IF) assay. In detail, $1*10^6$ of cells were fixed using formaldehyde 4% in PBS1X for 15 minutes at 4°C. Cells were washed and permeabilized with Triton 0.1X in PBS1X for 10 minutes at room temperature. Subsequently, cells were incubated with LCK antibody (CS2657, Cell Signaling Technology) diluted 1:100 in PBS1X overnight at 4°C. Cells were washed and incubated with an Alexa Fluor 594 goat anti-mouse IgG secondary antibody (Thermo Fisher Scientific, Cat # A11032, RRID: AB_2534091) diluted 1:200 in PBS1X for 30 minutes at room temperature. Cells were analyzed through the Zeiss LSM800 Airyscan microscope. The LCK median fluorescence intensity for each image of ALL-SIL and TALL-1 ShRNA *NFATc1* knock-down and controls was calculated using the ImageJ software.

Flow Cytometry analysis

CD4 staining was performed in ALL-SIL and TALL-1 ShRNA *NFATc1* knock-down cells and in the control, incubating $5*10^5$ the cells with 10 µL of the CD4 (SK3) FITC (BD345768, Beckton Dickinson, Franklin Lakes, NJ, USA) for 20 minutes at room temperature in the dark. $5*10^5$ RPMI-8402 ShRNA *NFATc2* knock down cells and controls were stained with a 10 µL of antibody mix (CD34 APC-A Becton Dickinson (BD), NJ, USA, Cat# 345804; CD7 PC5-5A Beckman Coulter (BC) CA, USA, Cat# IM3613; CD45 APC-A750-A, BD Cat# 348815; CD3 K0525-A, BC Cat# B00068; CD19 PB450-A, BC Cat# B49213; CD5 PC7-A, BD Cat# 348810; CD4 FITC-A, BD Cat# 345768; CD8 PE-A, BD Cat# 345773) for 30 minutes at room temperature in the dark. $5*10^5$ TALL-1 ShRNA *NFATc1* knock-down cells and controls were stained with a 10 µL of antibody mix (CD4 FITC-A, BD Cat# 340422; CD8 PE-A, BD Cat# 555367; CD5 PeCy5-A, BD Cat# 555354; CD34 PeCy7-A, BD Cat# 34879; CD45 APC-A750-A, BD Cat# 348795; CD19 APC-A, BD Cat# 340722; CD3 K0525-A, BC Cat# B00068) for 30 minutes at room temperature in the dark. After washing, cells were analyzed through Cytoflex Beckman Coulter. Intensity Fluorescence analyses were performed by FlowJo v7.6.5.

Reference:

[1] Bachmann PS, Gorman R, Papa RA, et al. Divergent mechanisms of glucocorticoid resistance in experimental models of pediatric acute lymphoblastic leukemia. *Cancer Res*. 2007;1;67(9):4482-90.

[2] Haferlach T, Kohlmann A, Wieczorek L, et al. Clinical utility of microarray-based gene expression profiling in the diagnosis and subclassification of leukemia: report from the International Microarray Innovations in Leukemia Study Group. *J Clin Oncol.* 2010;28(15):2529-37

[3] Pinazza M, Borga C, Agnusdei V, et al. An immediate transcriptional signature associated with response to the histone deacetylase inhibitor Givinostat in T acute lymphoblastic leukemia xenografts. *Cell Death Dis.* 2016;6(1):e2047.

[4] Dong X, Ding L, Thrasher A, et al. NetBID2 provides comprehensive hidden driver analysis. *Nat Commun*. 2023;14(1):2581.

[5] Stoletov K, Montel V, Lester RD, Gonias SL, Klemke R. High-resolution imaging of the dynamic tumor cell vascular interface in transparent zebrafish. *Proc Natl Acad Sci U S A.* 2007;104(44):17406-11.

[6] Kimmel CB, Ballard WW, Kimmel SR, Ullmann B, Schilling TF. Stages of embryonic development of the zebrafish. *Dev Dyn*. 1995;203(3):253-310.

[7] Mariotto E, Rampazzo E, Bortolozzi R, et al. Molecular and functional profiling of chemotolerant cells unveils nucleoside metabolism-dependent vulnerabilities in medulloblastoma. *Acta Neuropathol Commun.* 2023;11(1):183.

[8] Serafin V, Porcù E, Cortese G, et al. SYK Targeting Represents a Potential Therapeutic Option for Relapsed Resistant Pediatric *ETV6-RUNX1* B-Acute Lymphoblastic Leukemia Patients. *Int J Mol Sci.* 2019;20(24):6175.

[9] Visigalli I, Ungari S, Martino S, et al. The galactocerebrosidase enzyme contributes to the maintenance of a functional hematopoietic stem cell niche. *Blood.* 2010;116(11):1857-66.

[10] Veltri G, Silvestri C, Gallingani I, et al. Ruxolitinib as a Novel Therapeutic Option for Poor Prognosis T-LBL Pediatric Patients. *Cancers (Basel).* 2021;13(15):3724.

[11] Rossi T, Zamponi R, Chirico M, et al. BETi enhance ATGL expression and its lipase activity to exert their antitumoral effects in triple-negative breast cancer (TNBC) cells. J *Exp Clin Cancer Res.* 2023;42(1):7.

[12] Ntziachristos P, Tsirigos A, Van Vlierberghe P, et al. Genetic inactivation of the polycomb repressive complex 2 in T cell acute lymphoblastic leukemia. *Nat Med*. 2012;18(2):298-301.

[13] Bucher P, Erdmann T, Grondona P, et al. Targeting chronic NFAT activation with calcineurin inhibitors in diffuse large B-cell lymphoma. *Blood*. 2020;135(2):121-132.